Diachronous post-orogenic magmatism within a developing orocline in Iberia, European Variscides

Gabriel Gutiérrez-Alonso,[1] Javier Fernández-Suárez,[2] Teresa E. Jeffries,[3] Stephen T. Johnston,[4] Daniel Pastor-Galán,[1] J. Brendan Murphy,[5] M. Piedad Franco,[1] and J. Carlos Gonzalo[1]

Received 18 November 2010; revised 7 June 2011; accepted 14 July 2011; published 8 October 2011.

[1] U-Pb (zircon) crystallization ages of 52 late-Variscan granitoid intrusions from NW Iberia (19 from new data, 33 from previous studies) constrain the lithospheric evolution of this realm of the Variscan belt of Western Europe and allow assessment of the relationship between oroclinal development and magmatism in late-Carboniferous-early Permian times. The U-Pb ages, in conjunction with a range of geological observations, are consistent with the following sequence of events: (i) oroclinal bending starts at 310–305 Ma producing lithospheric thinning and asthenospheric upwelling in the outer arc of the orocline accompanied by production of mantle and lower crustal melts; (ii) between 305 and 300 Ma, melting continues under the outer arc of the orocline (Central Iberian Zone of the Iberian Variscan belt) and mid-crustal melting is initiated. Coevally, the lithospheric root beneath the inner arc of the orocline thickened due to progressive arc closure; (iii) between 300 and 292 Ma, foundering of the lithospheric root followed by melting in the lithospheric mantle and the lower crust beneath the inner arc due to upwelling of asthenospheric mantle; (iv) cooling of the lithosphere between 292 and 286 Ma resulting in a drastic attenuation of lower crustal high-temperature melting. By 285 Ma, the thermal engine generated by orocline-driven lithospheric thinning/delamination had cooled down beyond its capability to produce significant amounts of mantle or crustal melts. The model proposed explains the genesis of voluminous amounts of granitoid magmas in post-orogenic conditions and suggests that oroclines and similar post-orogenic granitoids, common constituents of numerous orogenic belts, may be similarly related elsewhere.

Citation: Gutiérrez-Alonso, G., J. Fernández-Suárez, T. E. Jeffries, S. T. Johnston, D. Pastor-Galán, J. B. Murphy, M. P. Franco, and J. C. Gonzalo (2011), Diachronous post-orogenic magmatism within a developing orocline in Iberia, European Variscides, *Tectonics*, *30*, TC5008, doi:10.1029/2010TC002845.

1. Introduction

[2] Growth and recycling of continental crust occur mainly at convergent plate boundaries [*Whitmeyer and Karlstrom*, 2007]; recycling primarily occurs through (i) the subduction of continent-derived sediments [*Rapp et al.*, 2008], and (ii) melting of the lower-middle crust [*Caldwell et al.*, 2009; *Depine et al.*, 2008]. Crustal growth occurs through the addition of melts that originate in the sub-continental lithospheric mantle [*Song et al.*, 2008] or the asthenospheric mantle [*Beccaluva et al.*, 2007]. Therefore the study of magmatism in subduction, collisional and post-orogenic environments is key to further our understanding of continental lithospheric evolution in time and space [*Murphy and Dostal*, 2007].

[3] The first-order connection between granitoid magmatism and tectonic environment is widely recognized [*Barbarin*, 1999; *Pearce et al.*, 1984; *Pitcher*, 1979]. However, granitoid rocks exhibit widely varying geochemical and isotopic characteristics, and the origin of this variability is controversial [e.g., *Pitcher*, 1979]. Among the granitoids generated in convergent continental settings, the genesis of post-orogenic granitoids is poorly understood [*Bonin*, 2004], possibly because they commonly display "hybrid" geochemical and isotopic signatures between archetypical I-type subduction-related and syn-collisional S-type (leuco)granitoids, [*Roberts and Clemens*, 1993; *Villaseca et al.*, 2009; *Williamson et al.*, 1996].

[4] Understanding the petrogenesis of post-orogenic granites requires knowledge of (i) their age and regional geologic setting, (ii) the composition of potential litho-

[1]Departamento de Geología, Universidad de Salamanca, Salamanca, Spain.
[2]Departemento de Petrología y Geoquímica, Universidad Complutense and IGEO-CSIC, Madrid, Spain.
[3]Department of Mineralogy, Natural History Museum, London, UK.
[4]School of Earth and Ocean Sciences, University of Victoria, Victoria, British Columbia, Canada.
[5]Department of Earth Science, St. Francis Xavier University, Antigonish, Nova Scotia, Canada.

Copyright 2011 by the American Geophysical Union.
0278-7407/11/2010TC002845

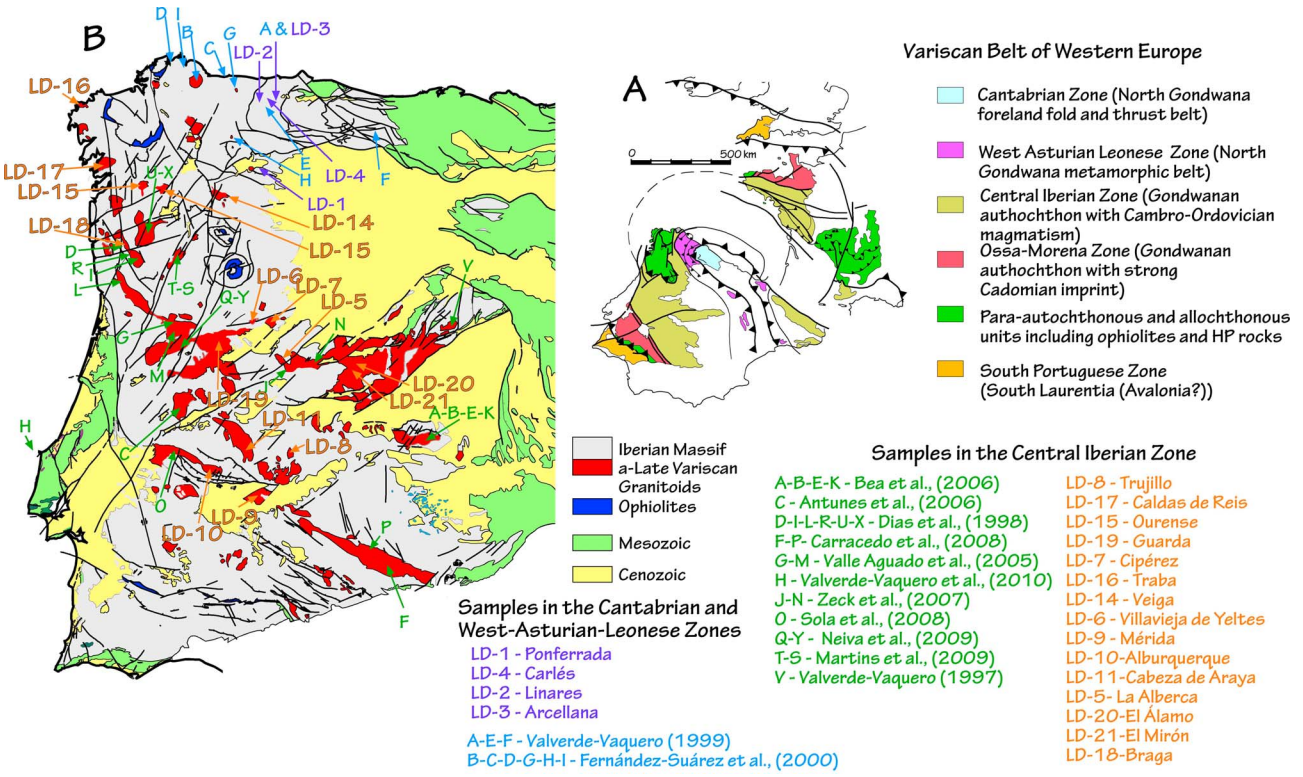

Figure 1. (a) Geologic sketch of Western Europe where the different Variscan tectonostratigraphic units depict the Iberian Armorican Arc. (b) Location of the post-orogenic granitoid plutons in western Iberia with indication of the samples studied and the U-Pb geochronological data from the literature.

spheric sources involved in melting, and (iii) the regional thermal regime. In Iberia, Late Carboniferous-Early Permian post-orogenic granitoid rocks are abundant and their extrusive equivalents have been documented within the Paleozoic Variscan orogenic belt of Western Europe [*Wilson et al.*, 2004]. Variscan orogenesis resulted from the collision between Laurasia and Gondwana forming Pangea. Iberia was located in the interior of Pangea at the time of post-orogenic granitoid intrusion [*Gutiérrez-Alonso et al.*, 2008b].

[5] The building and extensional collapse of the main orogenic edifice in Iberia was completed by ca. 320 Ma [*Bea et al.*, 2006; *Castiñeiras et al.*, 2008; *Valverde-Vaquero et al.*, 2006] and a syn-tectonic granitoid suite (ca. 325–315 Ma) was coeval with crustal thickening and subsequent extension [*Dias et al.*, 1998; *Fernández-Suárez et al.*, 2000]. In NW Iberia, there was a later magmatic pulse between ca. 310 and 290 Ma, post-dating the main orogenic tectonic events by 15 to 30 My [*Bea et al.*, 2006; *Castiñeiras et al.*, 2008; *Valverde-Vaquero et al.*, 2006]. This magmatic event generated large volumes of granitoid magmas (Figure 1) and subordinate amounts of mafic rocks intruding across the orogenic hinterland and, unusually, into the foreland fold and thrust belt. Emplacement of a large volume of igneous rocks (which are the object of this study) that cut across the penetrative Variscan structures, fabrics and structural grain [*Aranguren et al.*, 2003; *Yenes et al.*, 1999] 15 Ma after the end of Variscan orogenesis implies the existence of first-order, lithospheric-scale processes in the aftermath of Variscan collisional orogenesis that resulted in widespread melting.

[6] In most orogens, post-orogenic magmatism preferentially occurs in the upper (overriding) plate and has been interpreted to be caused by the break-off of the subducting plate and related asthenospheric upwelling [*Davies and Von Blanckenburg*, 1995]. In contrast, post-orogenic magmatism in the Iberian portion of the Variscan belt occurred in the lower plate [*Johnston and Gutiérrez-Alonso*, 2010].

[7] Several models have been put forward to explain the post-orogenic (i.e., "late-Variscan") igneous pulse in NW Iberia, including (i) radiogenic heat production in a thickened crust [*Bea et al.*, 2003]; (ii) the presence of a mantle plume [*Pinarelli and Rottura*, 1995] and (iii) delamination of a thickened lithospheric root [*Fernández-Suárez et al.*, 2000].

[8] A first-order tectonic event broadly coeval with the post-orogenic magmatism in NW Iberia is the oroclinal bending of the initially linear Variscan belt into a horseshoe shape, generating the Iberian-Armorican Arc (IAA), which took place between ca. 310 and 300 Ma [*Weil et al.*, 2001, 2010]. Oroclines are common feature in many orogenic belts and play a significant role in the development of their final geometry. Oroclines have been described elsewhere along the geologic record (i.e., the Alaskan orocline [*Johnston*, 2001]; the Bolivian orocline [*Allmendinger et al.*, 2005]; the Carpathians [*Fillerup et al.*, 2010]) and some of them were developed coevally with the IAA during the amalgamation of Pangea (e.g., the Tuva-Mongol orocline [*Levashova et al.*, 2003; *Şengör*, 1983; *Şengör and Natalin*, 1996]; the Kazakhstan orocline [*Abrajevitch et al.*, 2008]).

[9] Recent work has postulated a cause-effect relationship between the generation of the post-orogenic magmatism and the genesis of the IAA [*Gutiérrez-Alonso et al.*, 2004; *Weil et al.*, 2010], the whole process being driven by the special global geodynamic situation produced during the amalgamation of Pangea [*Gutiérrez-Alonso et al.*, 2008b].

[10] In order to test the potential relationship between the voluminous post-orogenic magmatism and the development of the IAA we have undertaken a study to determine the crystallization ages of granitoid and mafic post-orogenic plutons emplaced across the entire western Iberian section of the Variscan orogenic belt (Figure 1). For this purpose we dated 19 intrusions using U-Pb LA-ICPMS (zircon) and compiled the previously published U-Pb ages of rocks belonging to the post-orogenic suite. Our aim is to constrain the chronological and spatial distribution of these post-orogenic intrusions and in doing so, test models for the tectonic evolution of the region. In previous studies, the hypothesis of lithospheric delamination as a trigger for post-orogenic magmatism in NW Iberia has been postulated based on the evolution of Sm-Nd isotopic composition of mantle-derived rocks [*Gutiérrez-Alonso et al.*, 2011] and as a thermomechanical consequence of oroclinal bending of this section of the Variscan belt [*Gutiérrez-Alonso et al.*, 2004; *Weil et al.*, 2010]. In this study, the geochronological data are considered in combination with the regional tectono-stratigraphic zonation, and petrological-geochemical features of these rocks (see also *Fernández-Suárez et al.* [2000] and *Fernández-Suárez et al.* [2011] for detailed petrological and geochemical information) to test the potential connection between post-orogenic oroclinal bending of the belt and post-orogenic magmatism. This test, to be successful, requires that the locus and age of granitoid magma genesis be consistent with the thermomechanical evolution of a bending lithosphere. In this study, we provide the most detailed chronology available to date on the crystallization ages of the different post-orogenic granitoid types across the NW Iberian Variscan belt and use this chronological information to propose a mechanism whereby these granitoids were produced in a post-orogenic environment by orocline-triggered lithospheric delamination/thinning.

2. Geological Setting

[11] The Iberian Massif, which constitutes the extensive outcrop of Paleozoic and Ediacaran rocks in western Iberia (Figure 1), is part of the Variscan orogen of Western Europe. The Variscan orogen was contiguous with the Appalachian-Ouchita orogen of North America before the Mesozoic opening of the Atlantic Ocean [*Nance et al.*, 2010]. The Iberian massif is underlain by Proterozoic Gondwanan basement of Cadomian (West African) and Avalonian (Amazonian) affinities, which provides the foundation for an Ediacaran subduction-related basin and Palaeozoic, mostly siliciclastic, passive margin sequences that are characteristic of the northern Gondwanan margin [*Fernández-Suárez et al.*, 2002; *Gutiérrez-Alonso et al.*, 2005; *Murphy et al.*, 2008; *Nance et al.*, 2010].

[12] The magmatic evolution of the Variscan orogen of Iberia includes: (i) A subduction-related Cadomian (ca. 600 Ma) magmatic event [*Fernández-Suárez et al.*, 1998] scarcely represented in NW Iberia mostly by I-type granitoid and volcanic rocks; (ii) a voluminous extension-related magmatic event in the Cambrian-Ordovician boundary (ca. 490–470 Ma) linked to the opening of the Rheic Ocean [*Bea et al.*, 2006; *Montero et al.*, 2007; *Montes et al.*, 2010; *Valverde-Vaquero and Dunning*, 2000]; (iii) Carboniferous syn-orogenic (Variscan) magmatism that began at ca. 350–340 Ma in the hinterland of the orogen [*Pérez-Estaún and Bea*, 2004] and ended at ca. 320–315 Ma [*Valle Aguado et al.*, 2005; *Dias et al.*, 1998; *Fernández-Suárez et al.*, 2000]; (iv) post-orogenic magmatism that peaked at ca. 310–295 Ma when voluminous mafic and granitoid magmas and extrusive equivalents were emplaced and erupted in both the internal and external zones of the orogen [*Bea et al.*, 2006; *Lago et al.*, 2004; *Moreno-Ventas et al.*, 1995; *Orejana et al.*, 2009], including the foreland fold-and-thrust belt [*Fernández-Suárez et al.*, 2000] (Figure 1).

[13] The main features/events of the Variscan orogen can be summarized as follows: The northern Gondwanan margin formed the southern flank of the Rheic Ocean and the closure of this ocean is recorded in the Iberian massif by the Laurussia-Gondwana collision (the Variscan orogeny). Ocean closure began by 400 Ma as indicated by subduction-related metamorphism of the Laurussian margin of the Rheic Ocean [*Gómez Barreiro et al.*, 2006; *Fernández-Suárez et al.*, 2007; *Ibarguchi et al.*, 1990; *Martínez Catalán et al.*, 2009; *Mendía Aranguren*, 2000]. The subduction, at 395 Ma, of the Rheic mid-oceanic ridge beneath the Laurentian margin [*Gutiérrez-Alonso et al.*, 2008a; *Woodcock et al.*, 2007] may explain the subsequent increase in the convergence rate and the coupling of both oceanic margins. Remnants of the Rheic Ocean lithosphere are preserved in the ophiolites that characterize the suture zones along which the continents are juxtaposed [*Arenas et al.*, 2007; *Martínez Catalán et al.*, 1997] (Figure 1).

[14] The Iberian record of continental collision began at ca. 365 Ma [*Dallmeyer and Ibarguchi*, 1990; *Rodríguez et al.*, 2003] when subduction of the outermost continental margin of Gondwana beneath Laurentia commenced. The resulting deformation front migrated east as the upper plate (Laurussia) was thrust onto the lower plate (Gondwana), imbricating and folding the extensive Gondwanan passive margin stratigraphic sequence [*Martínez Catalán et al.*, 2007; *Dallmeyer et al.*, 1997; *Martínez Catalán et al.*, 2009].

[15] Convergence initially produced east verging recumbent folds that migrated east, toward the present-day core of the IAA (D1 deformation). Increasing shortening and thickening lead to the extensional collapse (D2 deformation) of the thickened hinterland [*Arenas and Catalan*, 2003; *Diez Balda et al.*, 1995; *Bastida et al.*, 2010; *Martínez Catalán et al.*, 2003; *Viruete et al.*, 1994] at ca. 320 Ma [*Martínez Catalán et al.*, 2009], coeval with the initiation of the non-metamorphic foreland-verging fold and thrust belt (the Cantabrian Zone [*Alonso et al.*, 2009; *Pérez-Estaún et al.*, 1994]). Late stage collision-related deformation included development of large wavelength upright folds (D3 deformation) and strike-slip ductile shear zones [*Martínez Catalán et al.*, 2009]. Immediately after the building of the Variscan orogen, a 180° rotation of the mountain chain, documented by paleomagnetic data, led to the formation of the Iberian-Armorican Arc (IAA) [*Gutiérrez-Alonso et al.*, 2008b; *Weil et al.*, 2010], an event requiring a dramatic change in the stress-strain field acting on the core of Pangea. The IAA

formation was accompanied by orogen-scale thermal activity that is interpreted to have been caused by a coeval late Carboniferous-early Permian lithospheric delamination event [*Fernández-Suárez et al.*, 2000; *Gutiérrez-Alonso et al.*, 2004, 2008b; *Weil et al.*, 2001, 2010].

3. Geochronological Methods

[16] Samples were crushed with a jaw crusher and pulverized with a disc mill. Zircons were separated at the Salamanca and Complutense (Madrid) Universities by heavy fraction enrichment on a Wilfley table followed by density separation using di-iodomethane (CH_2I_2) and magnetic separation in a Frantz isodynamic separator. Zircons were selected from the least magnetic fraction and hand-picked in alcohol under a binocular microscope. Zircon grains were set in synthetic resin mounts, polished to approximately half their thickness and cleaned in a warm HNO_3 ultrasonic bath. U-Pb dating of zircon was conducted at the analytical facilities of The Natural History Museum, London. Analytical instrumentation consisted of a UP193FX excimer laser ablation system (NewWave Research, Fremont, USA) coupled to a 7500cs, quadrupole based ICP-MS instrument (Agilent Technologies). Analytical conditions used for individual zircon analyses are those given in [*Jeffries et al.*, 2003].

[17] Samples and standard were ablated in an air-tight sample chamber flushed with Helium for sample transport. The laser was focused on the sample surface and energy density was kept constant for each analysis. The samples were rastered along lines ca. 25 to 50 microns long (depending on zircon size), using a constant raster speed for each analysis. Nominal beam diameter was 30 μm for zircon analyses.

[18] Data were collected in discrete runs of 20 analyses, comprising 12 unknowns bracketed before and after by 4 analyses of the standard zircon 91500 [*Wiedenbeck et al.*, 1995]. During the analytical sessions of samples the standard 91500 yielded a weighted average (n = 160) of 1062.8 ± 1.8 Ma (MSWD = 1.06) for the $^{206}Pb/^{238}U$ age (certified ID-TIMS $^{206}Pb/^{238}U$ age: 1062.4 ± 0.4 Ma) and a weighted average of 1064.5 ± 2.6 Ma (MSWD = 0.9) for the $^{207}Pb/^{206}Pb$ age (certified ID-TIMS $^{207}Pb/^{206}Pb$ age: 1065.4 ± 0.3 Ma).

[19] Data for sample zircons were collected for up to 135 s per analysis with a gas background taken during the initial 45 s. For each analysis, time-resolved signals were obtained and then studied to ensure that stable flat signal intervals were used in the age calculations. Preliminary selection of background and analysis signal intensities and data calculation were performed using 'LAMTRACE', a macro based spreadsheet written by Simon Jackson, Macquarie University, Australia. Background and mass bias corrected signal intensities and counting statistics were calculated for each isotope. Concordia age calculations, and concordia and cumulative probability plots were performed using Isoplot/Ex rev. three [*Ludwig*, 2003]. Data treatment, assignment of final ages and errors for individual analyses and criteria for rejection of analyses are those detailed by *Fernández-Suárez et al.* [2002] and *Jeffries et al.* [2003]. The latter paper also shows that crystallization ages for igneous rocks (derived from U-Pb analyses on magmatic zircon domains) obtained with this LA-ICPMS instrumentation and analytical protocol are indistinguishable from those obtained by ID-TIMS analyses on single grains of the same zircon populations.

4. Results

[20] Zircons from 19 samples of 19 post-orogenic plutons from the Variscan belt of NW Iberia (Figure 1) were analyzed and the results are given in Table 1 and in the concordia plots of Figures 2 and 3. The table and plots show the isotopic ratios and derived ages of those analyses that are concordant (i.e., analyses whose corresponding 2σ ellipses intercept the concordia curve). Since discordance in LA-ICP-MS analyses can be caused by any combination of i) lead loss, ii) analyses of mixed aged domains, iii) high common Pb; the discordant analyses are not further considered as corrections or assumptions do not warrant that the interpreted ages are correct.

[21] For each pluton a *Concordia Age* [*Ludwig*, 1998] has been generated (Figures 2 and 3) pooling the concordant analyses (Table 1) using Isoplot 3 [*Ludwig*, 2003]. The resulting age and error are taken to represent the best approximation to the crystallization/consolidation age of each intrusion.

[22] Precision of individual analyses in this study (usually >5 Ma for the $^{206}Pb/^{238}U$ age) precludes finer considerations on the significance of the spread of "magmatic" concordant ages (i.e., antecrysts versus autocrysts, see, for example, *Miller et al.* [2007]) but we are confident that the reported ages are sufficiently precise to be valid in the context of the discussion presented herein. Moreover, plutons that have been dated by ID-TIMS and LA-ICPMS yield ages that are analytically equivalent (e.g., Arcellana pluton [*Valverde-Vaquero et al.*, 1999], Table 2; see also *Jeffries et al.* [2003]). The same is true for plutons dated by SIMS and LA-ICPMS (this study) (e.g., Nisa-Alburquerque pluton [*Solá et al.*, 2009], Table 2). Note that the age reported for each pluton has been calculated in the same fashion for all samples (i.e., concordia age as defined by [*Ludwig*, 1998]) thus avoiding statistical age shifts that would result from using different approaches (e.g., weighted average of the $^{206}Pb/^{238}U$ ages, median $^{206}Pb/^{238}U$ age as calculated by the TuffZirc algorithm [*Ludwig*, 2003], upper or lower intercepts of discordia lines, projection from an assigned common lead composition on a Tera-Wasserburg Concordia plot, etc.).

[23] Additionally, we have compiled U-Pb age data (both ID-TIMS and SIMS) from the literature for post-orogenic plutons in Iberia (Table 2) which are used in the discussion below. In total, we utilize U-Pb age data from 52 late-Variscan discrete intrusions (19 from new data presented herein and 33 from previous geochronological works) (Figure 1 and Table 2).

[24] Within the data set, 13 U-Pb ages correspond to intrusions in the foreland and thrust belt of the Variscan Iberian belt (Cantabrian and West Asturian-Leonese zones, CZ + WALZ) and 39 correspond to intrusions the hinterland (Central Iberian Zone, CIZ) (Figure 1). The samples include gabbros, quartz-diorites, Bt ± Hbl peraluminous to slightly metaluminous granodiorites, peraluminous Bt ± Crd granodiorites and monzogranites, two-mica peraluminous monzogranites and peraluminous leucogranites with primary Ms ± Bt ± Grt ± Tur ± And ± Sil (Table 2). The main

Table 1. LA-ICP-MS U-Pb Results[a]

Pluton	Sample	Analysis Number	Isotopic Ratios and 2σ (%) Errors						Ages and 2σ Absolute Errors (Ma)					
			$^{206}Pb/^{238}U$	$\pm2\sigma$	$^{207}Pb/^{235}U$	$\pm2\sigma$	$^{207}Pb/^{206}Pb$	$\pm2\sigma$	$^{206}Pb/^{238}U$	$\pm2\sigma$	$^{207}Pb/^{235}U$	$\pm2\sigma$	$^{207}Pb/^{206}Pb$	$\pm2\sigma$
N42°33′39.0″	W006°33′26.3″													
Ponferrada	LD-1	oc13a11	0.0454	1.90	0.3211	3.68	0.0516	3.94	286	5	283	9	268	90
Ponferrada	LD-1	oc12b13	0.0456	1.44	0.3275	2.86	0.0519	2.70	287	4	288	7	282	62
Ponferrada	LD-1	oc13a08	0.0455	2.38	0.3305	4.42	0.0528	4.42	287	7	290	11	320	63
Ponferrada	LD-1	oc12b14	0.0457	1.34	0.3266	3.40	0.0522	2.58	288	4	287	8	292	58
Ponferrada	LD-1	oc12b16	0.0456	2.12	0.3239	3.90	0.0521	3.50	288	6	285	10	288	80
Ponferrada	LD-1	oc12b12	0.0461	1.22	0.3332	2.40	0.0521	2.14	291	3	292	6	290	50
Ponferrada	LD-1	oc13a16	0.0463	1.56	0.3308	4.40	0.0516	4.06	292	4	290	11	268	94
Ponferrada	LD-1	oc12b15	0.0465	1.32	0.3294	2.66	0.0515	2.30	293	4	289	7	264	54
Ponferrada	LD-1	oc12b07	0.0466	2.60	0.3393	3.42	0.0524	3.08	294	7	297	9	302	70
Ponferrada	LD-1	oc12b08	0.0468	1.42	0.3428	3.58	0.0530	3.02	295	4	299	9	328	68
											Concordia Age: 290.1 ± 1.4 Ma			
N43°14′10.6″	W006°33′34.3″													
Linares	LD-2	oc22e07	0.0469	2.74	0.3384	4.22	0.0523	5.88	296	8	296	11	298	134
Linares	LD-2	oc13b11	0.0472	1.80	0.3372	2.72	0.0519	2.58	297	5	295	7	282	58
Linares	LD-2	oc13b13	0.0472	1.46	0.3372	1.20	0.0531	1.66	297	4	295	3	332	38
Linares	LD-2	oc13c09	0.0472	2.20	0.3347	4.20	0.0523	3.86	297	6	293	11	296	88
Linares	LD-2	oc22f10	0.0476	1.82	0.3505	2.92	0.0535	3.82	300	5	305	8	348	86
Linares	LD-2	oc22f15	0.0478	1.84	0.3427	4.62	0.0516	5.12	301	5	299	12	264	118
Linares	LD-2	oc22f08	0.0479	3.10	0.3518	6.92	0.0527	5.30	302	9	306	18	316	120
											Concordia Age: 297.3 ± 1.8 Ma			
N43°23′19.3″	W006°15′15.4″													
Arcellana	LD-3	oc13e14	0.0462	1.60	0.3292	3.54	0.0522	3.68	291	5	289	9	290	84
Arcellana	LD-3	oc22h07	0.0462	2.12	0.3318	3.80	0.0526	3.68	291	6	291	10	310	84
Arcellana	LD-3	oc13e05	0.0466	2.12	0.3433	3.10	0.0529	2.48	294	6	300	8	322	56
Arcellana	LD-3	oc13d05	0.0471	1.90	0.3436	4.80	0.0527	4.28	297	6	300	12	314	98
Arcellana	LD-3	oc13e06	0.0472	1.78	0.3379	4.38	0.0515	3.44	297	5	296	11	260	80
Arcellana	LD-3	oc13d14	0.0476	1.48	0.3469	2.86	0.0538	2.68	300	4	302	7	362	60
Arcellana	LD-3	oc13d11	0.0480	1.50	0.3487	2.44	0.0531	2.08	302	4	304	6	332	48
											Concordia Age: 296.7 ± 2.9 Ma			
N43°21′33.4″	W006°14′54.8″													
Carles	LD-4	oc14b06	0.0459	2.32	0.3408	3.84	0.0541	3.66	289	7	298	10	374	82
Carles	LD-4	oc14a07	0.0461	1.14	0.3389	3.32	0.0534	3.00	291	3	296	9	344	68
Carles	LD-4	oc14b09	0.0462	1.66	0.3365	3.62	0.0531	3.82	291	5	295	9	332	86
Carles	LD-4	oc14a08	0.0464	2.00	0.3434	4.58	0.0538	3.94	292	6	300	12	360	88
Carles	LD-4	oc14b12	0.0463	1.60	0.3423	3.54	0.0536	3.54	292	5	299	9	352	80
Carles	LD-4	oc14a06	0.0467	1.20	0.3323	3.60	0.0523	2.98	294	3	291	9	296	68
Carles	LD-4	oc14b11	0.0475	1.52	0.3380	2.44	0.0525	2.74	299	4	296	6	308	62
											Concordia Age: 293.1 ± 2.4 Ma			
N40°32′07.4″	W006°08′54.3″													
La Alberca	LD-5	oc14c10	0.0486	0.92	0.3550	2.58	0.0532	2.34	306	3	309	7	336	52
La Alberca	LD-5	oc14c16	0.0488	1.38	0.3600	4.28	0.0531	4.48	307	4	312	12	332	100
La Alberca	LD-5	oc14c06	0.0490	1.62	0.3594	2.74	0.0534	2.92	308	5	312	7	342	66
La Alberca	LD-5	oc14c09	0.0491	0.96	0.3572	2.86	0.0532	2.62	309	3	310	8	336	60
La Alberca	LD-5	oc14c14	0.0493	0.88	0.3527	2.90	0.0523	2.44	310	3	307	8	296	56
La Alberca	LD-5	oc14c08	0.0494	1.68	0.3659	3.30	0.0523	3.42	311	5	317	9	298	78
											Concordia Age: 308.7 ± 1.4 Ma			
N40°53′16.6″	W006°28′14.7″													
Villavieja de Yeltes	LD-6	oc22c10	0.0475	2.48	0.3502	5.08	0.0532	5.24	299	7	305	18	338	118
Villavieja de Yeltes	LD-6	oc22c16	0.0481	2.14	0.3601	5.00	0.0533	7.24	303	6	312	24	330	152
Villavieja de Yeltes	LD-6	oc14e13	0.0483	1.66	0.3539	2.49	0.0534	1.88	304	6	308	8	344	42
Villavieja de Yeltes	LD-6	oc22d11	0.0485	2.92	0.3590	3.51	0.0545	4.35	305	9	313	9	342	88
Villavieja de Yeltes	LD-6	oc14f 07	0.0486	1.98	0.3439	2.04	0.0546	2.28	306	6	300	9	394	52
Villavieja de Yeltes	LD-6	oc14e06	0.0488	1.80	0.3651	4.42	0.0532	4.60	307	7	316	12	338	104
											Concordia Age: 303.8 ± 2.3 Ma			
N40°56′21.6″	W006°13′55.0″													
Ciperez	LD-7	oc15b08	0.0467	1.78	0.3436	3.84	0.0532	3.02	294	5	300	10	338	68
Ciperez	LD-7	oc15b12	0.0466	2.30	0.3418	4.12	0.0534	4.36	294	7	299	11	344	98
Ciperez	LD-7	oc23a05	0.0471	1.80	0.3413	3.16	0.0527	2.76	296	5	298	8	314	62
Ciperez	LD-7	oc23b15	0.0471	2.26	0.3508	7.08	0.0549	6.40	297	7	305	19	408	144
Ciperez	LD-7	oc15b11	0.0473	1.54	0.3372	5.02	0.0515	4.34	298	4	295	13	264	98
Ciperez	LD-7	oc23a13	0.0473	2.18	0.3502	4.32	0.0536	4.76	298	6	305	11	352	106

Table 1. (continued)

Pluton	Sample	Analysis Number	Isotopic Ratios and 2σ (%) Errors						Ages and 2σ Absolute Errors (Ma)					
			$^{206}Pb/^{238}U$	$\pm2\sigma$	$^{207}Pb/^{235}U$	$\pm2\sigma$	$^{207}Pb/^{206}Pb$	$\pm2\sigma$	$^{206}Pb/^{238}U$	$\pm2\sigma$	$^{207}Pb/^{235}U$	$\pm2\sigma$	$^{207}Pb/^{206}Pb$	$\pm2\sigma$
Ciperez	LD-7	oc23a08	0.0485	1.22	0.3453	2.72	0.0525	2.58	305	4	301	7	306	58
Ciperez	LD-7	oc23a10	0.0487	1.66	0.3514	3.32	0.0518	3.82	307	5	306	9	274	88
											Concordia Age: 300 ± 2.9 Ma			
N39°31′44.2″	W005°53′06.7″													
Trujillo	LD-8	oc15c14	0.0462	1.86	0.3437	3.38	0.0535	3.44	291	5	300	9	348	78
Trujillo	LD-8	oc15c07	0.0463	2.14	0.3424	5.98	0.0538	6.26	292	6	299	16	360	140
Trujillo	LD-8	oc15c15	0.0471	2.02	0.3402	5.26	0.0519	4.88	297	6	297	14	280	112
Trujillo	LD-8	oc15c11	0.0478	1.70	0.3421	1.61	0.0532	1.72	301	5	300	4	334	38
											Concordia Age: 296.2 ± 2.5 Ma			
N38°56′50.4″	W006°26′28.0″													
Merida	LD-9	oc15f15	0.0468	3.60	0.3439	2.86	0.0534	5.52	295	10	300	7	344	126
Merida	LD-9	oc15f06	0.0471	2.82	0.3414	6.86	0.0523	6.16	297	8	298	18	296	140
Merida	LD-9	oc15d13	0.0477	2.10	0.3485	4.65	0.0536	3.72	300	3	304	6	352	84
Merida	LD-9	oc15e05	0.0479	2.24	0.3486	4.06	0.0525	3.00	301	7	304	11	306	68
Merida	LD-9	oc15f13	0.0478	1.34	0.3475	3.00	0.0528	3.02	301	4	303	8	320	68
Merida	LD-9	oc15e11	0.0489	1.12	0.3586	3.90	0.0531	3.36	308	3	311	10	330	76
Merida	LD-9	oc15d06	0.0491	1.50	0.3562	2.36	0.0528	1.90	309	5	309	6	318	44
Merida	LD-9	oc15e10	0.0493	1.36	0.3604	3.96	0.0532	3.60	310	4	312	11	338	82
Merida	LD-9	oc15f11	0.0493	1.70	0.3664	3.56	0.0542	2.70	310	5	317	10	378	60
											Concordia Age: 305.5 ± 2.5 Ma			
N39°13′31.3″	W006°59′55.7″													
Alburquerque	LD-10	oc16a08	0.0478	2.09	0.3439	4.25	0.0523	2.46	301	3	300	8	296	56
Alburquerque	LD-10	oc16a15	0.0480	1.54	0.3521	5.62	0.0530	5.50	302	5	306	15	328	124
Alburquerque	LD-10	oc16b10	0.0479	1.70	0.3421	3.42	0.0520	3.68	302	5	299	9	282	84
Alburquerque	LD-10	oc16a13	0.0481	1.02	0.3425	1.74	0.0535	1.58	303	3	299	5	350	36
Alburquerque	LD-10	oc16b14	0.0484	1.90	0.3416	4.40	0.0514	4.12	304	6	298	11	256	96
Alburquerque	LD-10	oc16h09	0.0486	1.74	0.3615	3.88	0.0537	3.74	306	5	313	10	358	84
Alburquerque	LD-10	oc16a07	0.0488	1.36	0.3477	3.16	0.0522	3.32	307	4	303	8	292	74
Alburquerque	LD-10	oc16a11	0.0487	1.94	0.3515	4.36	0.0517	4.14	307	6	306	11	272	94
Alburquerque	LD-10	oc16b06	0.0488	1.82	0.3557	2.40	0.0534	3.22	307	5	309	6	344	72
Alburquerque	LD-10	oc16b08	0.0487	2.36	0.3556	3.40	0.0529	2.84	307	7	309	9	322	64
Alburquerque	LD-10	oc16h05	0.0488	1.74	0.3627	4.20	0.0535	3.86	307	5	314	11	348	88
Alburquerque	LD-10	oc16a05	0.0489	1.08	0.3545	2.24	0.0524	2.50	308	3	308	6	302	58
Alburquerque	LD-10	oc16b07	0.0495	1.28	0.3601	2.02	0.0527	2.12	311	4	312	5	316	48
Alburquerque	LD-10	oc16h12	0.0497	1.78	0.3567	2.62	0.0528	2.70	313	5	310	7	320	60
											Concordia Age: 305.9 ± 1.6 Ma			
N39°33′05.6″	W006°26′18.9″													
Cabeza de Araya	LD-11	oc16d05	0.0488	1.78	0.3490	3.26	0.0514	2.86	307	5	304	9	258	66
Cabeza de Araya	LD-11	oc16c11	0.0490	1.98	0.3583	3.46	0.0530	3.18	308	6	311	9	326	72
Cabeza de Araya	LD-11	oc16d12	0.0489	1.54	0.3596	3.30	0.0532	3.02	308	5	312	9	338	70
Cabeza de Araya	LD-11	oc16d16	0.0490	2.08	0.3537	2.52	0.0527	3.06	308	6	308	7	316	70
Cabeza de Araya	LD-11	oc16c09	0.0491	1.18	0.3502	3.16	0.0516	3.26	309	4	305	8	268	74
Cabeza de Araya	LD-11	oc16c06	0.0495	2.36	0.3633	2.76	0.0538	3.06	311	7	315	7	362	68
Cabeza de Araya	LD-11	oc16c05	0.0496	1.98	0.3481	4.30	0.0512	4.18	312	6	303	11	250	96
Cabeza de Araya	LD-11	oc16d06	0.0496	2.52	0.3565	3.40	0.0526	4.28	312	8	310	9	310	98
Cabeza de Araya	LD-11	oc16d11	0.0497	1.72	0.3560	3.88	0.0521	3.22	313	5	309	10	288	74
											Concordia Age: 309.4 ± 1.7 Ma			
N42°14′39.9″	W007°01′39.8″													
Veiga	LD-14	oc19d06	0.0465	2.32	0.3405	4.84	0.0528	4.64	293	7	298	12	318	106
Veiga	LD-14	oc19f15	0.0466	1.98	0.3351	2.90	0.0521	2.60	293	6	293	7	288	58
Veiga	LD-14	oc19e15	0.0470	2.30	0.3391	4.14	0.0529	3.72	296	7	296	11	324	84
Veiga	LD-14	oc19f13	0.0481	2.62	0.3494	4.02	0.0540	3.16	303	8	304	11	370	70
Veiga	LD-14	oc19f12	0.0483	2.26	0.3426	3.58	0.0519	2.60	304	7	299	9	278	60
Veiga	LD-14	oc19e05	0.0484	1.44	0.3445	2.04	0.0521	2.36	305	4	301	5	288	54
Veiga	LD-14	oc19f09	0.0485	1.62	0.3487	2.50	0.0522	2.36	305	5	304	7	292	54
Veiga	LD-14	oc19e08	0.0488	2.02	0.3557	3.00	0.0530	2.64	307	6	309	8	330	60
Veiga	LD-14	oc19f05	0.0493	2.48	0.3523	4.00	0.0525	3.52	310	8	306	11	306	80
											Concordia Age: 301.9 ± 2.8 Ma			
N42°18′16.0″	W007°52′35.1″													
Orense	LD-15	oc19h08	0.0463	1.74	0.3407	3.42	0.0529	3.38	291	5	298	9	324	76
Orense	LD-15	oc19g05	0.0464	2.30	0.3351	6.84	0.0523	7.08	293	7	293	17	298	162
Orense	LD-15	oc19g07	0.0467	2.22	0.3337	5.96	0.0520	4.24	294	6	292	15	286	98
Orense	LD-15	oc19h07	0.0469	3.08	0.3465	4.62	0.0526	3.88	296	9	302	12	312	88
Orense	LD-15	oc19j06	0.0472	1.88	0.3467	3.62	0.0525	3.22	297	5	302	9	304	74

Table 1. (continued)

Pluton	Sample	Analysis Number	Isotopic Ratios and 2σ (%) Errors						Ages and 2σ Absolute Errors (Ma)					
			$^{206}Pb/^{238}U$	$\pm2\sigma$	$^{207}Pb/^{235}U$	$\pm2\sigma$	$^{207}Pb/^{206}Pb$	$\pm2\sigma$	$^{206}Pb/^{238}U$	$\pm2\sigma$	$^{207}Pb/^{235}U$	$\pm2\sigma$	$^{207}Pb/^{206}Pb$	$\pm2\sigma$
Orense	LD-15	oc19h16	0.0473	1.86	0.3562	5.56	0.0533	5.06	298	5	309	15	338	114
Orense	LD-15	oc19h12	0.0475	2.06	0.3438	3.96	0.0523	3.70	299	6	300	10	298	84
Orense	LD-15	oc19h13	0.0480	2.18	0.3452	6.12	0.0528	4.42	302	6	301	16	320	100
Orense	LD-15	oc19g06	0.0482	3.12	0.3426	5.62	0.0537	6.88	303	9	299	15	358	154
Orense	LD-15	oc19h11	0.0483	2.74	0.3457	4.76	0.0510	6.34	304	8	301	12	240	146
											Concordia Age: 297.5 ± 1.9 Ma			
N43°11′13.1″	W009°05′23.9″													
Traba	LD-16	oc22a05	0.0472	1.90	0.3336	3.00	0.0522	3.38	298	6	292	8	292	76
Traba	LD-16	oc20c07	0.0475	1.22	0.3396	3.06	0.0512	2.68	299	4	297	8	248	62
Traba	LD-16	oc20b12	0.0476	3.08	0.3569	4.92	0.0556	5.48	300	9	310	13	434	122
Traba	LD-16	oc22a06	0.0477	2.80	0.3388	3.18	0.0505	2.76	301	8	296	8	218	64
Traba	LD-16	oc22a14	0.0480	2.64	0.3423	4.67	0.0520	6.34	302	8	299	19	286	144
Traba	LD-16	oc22a07	0.0487	2.78	0.3410	4.75	0.0523	4.44	306	8	295	12	296	102
Traba	LD-16	oc20b05	0.0490	3.48	0.3539	2.84	0.0529	4.44	308	10	308	8	324	100
Traba	LD-16	oc22a09	0.0493	3.04	0.3492	4.02	0.0515	2.76	311	9	304	11	260	64
Traba	LD-16	oc22b05	0.0496	3.44	0.3545	4.48	0.0520	4.62	312	11	308	12	286	106
											Concordia Age: 301.2 ± 2.9 Ma			
N42°35′40.8″	W008°40′37.3″													
Caldas de Reis	LD-17	oc20d14	0.0464	1.72	0.3340	2.69	0.0524	2.00	292	2	293	5	302	46
Caldas de Reis	LD-17	oc20d15	0.0464	2.14	0.3346	6.70	0.0519	6.14	292	6	293	17	280	140
Caldas de Reis	LD-17	oc20d09	0.0465	1.36	0.3418	2.14	0.0526	2.38	293	4	299	6	308	54
Caldas de Reis	LD-17	oc20f05	0.0465	2.68	0.3450	5.10	0.0532	5.88	293	8	301	13	338	132
Caldas de Reis	LD-17	oc20e06	0.0468	2.26	0.3405	4.56	0.0527	4.74	295	6	298	12	314	108
Caldas de Reis	LD-17	oc20e07	0.0468	1.58	0.3347	3.90	0.0521	4.52	295	5	293	10	288	104
Caldas de Reis	LD-17	oc20e11	0.0468	1.50	0.3523	6.96	0.0540	5.12	295	4	306	18	372	116
Caldas de Reis	LD-17	oc20f09	0.0468	2.22	0.3449	4.40	0.0535	3.70	295	6	301	11	348	84
Caldas de Reis	LD-17	oc20e12	0.0469	1.64	0.3474	4.02	0.0540	3.96	296	5	303	11	370	88
Caldas de Reis	LD-17	oc20e13	0.0473	1.46	0.3375	4.76	0.0513	3.54	298	4	295	12	252	82
Caldas de Reis	LD-17	oc20f07	0.0476	1.50	0.3419	7.44	0.0513	6.16	300	4	299	19	254	142
Caldas de Reis	LD-17	oc20f08	0.0476	2.68	0.3522	6.80	0.0538	6.72	300	8	306	18	360	152
Caldas de Reis	LD-17	oc20f11	0.0477	2.52	0.3357	6.20	0.0511	5.96	300	7	294	16	246	138
Caldas de Reis	LD-17	oc20f16	0.0477	2.50	0.3442	4.98	0.0523	2.94	300	7	300	13	298	68
Caldas de Reis	LD-17	oc20e09	0.0479	1.82	0.3404	4.02	0.0518	4.30	301	5	297	10	276	98
Caldas de Reis	LD-17	oc20f15	0.0478	3.04	0.3330	4.08	0.0516	4.30	301	9	292	10	266	98
Caldas de Reis	LD-17	oc20d10	0.0479	2.34	0.3318	5.74	0.0515	5.12	302	7	291	15	262	118
Caldas de Reis	LD-17	oc20e10	0.0479	1.64	0.3566	4.02	0.0538	4.60	302	5	310	11	360	104
											Concordia Age: 297.1 ± 1.4 Ma			
N41°33′36.2″	W008°25′43.2″													
Braga	LD-18	oc20j05	0.0480	2.60	0.3482	4.64	0.0519	5.72	302	8	303	12	278	130
Braga	LD-18	oc20g16	0.0481	2.36	0.3573	5.66	0.0536	6.34	303	7	310	15	352	142
Braga	LD-18	oc20h06	0.0481	2.38	0.3449	3.20	0.0528	3.68	303	7	301	8	320	84
Braga	LD-18	oc20j16	0.0483	1.84	0.3598	3.52	0.0533	2.70	304	5	312	9	342	62
Braga	LD-18	oc20g09	0.0485	2.02	0.3653	5.44	0.0551	6.02	306	6	316	15	416	134
Braga	LD-18	oc20h10	0.0485	1.78	0.3479	4.50	0.0529	3.90	306	5	303	12	322	88
Braga	LD-18	oc20h05	0.0488	3.70	0.3658	7.78	0.0536	8.46	307	11	317	21	354	192
Braga	LD-18	oc20h14	0.0489	2.78	0.3419	5.68	0.0505	5.70	308	8	299	15	216	132
Braga	LD-18	oc20g12	0.0490	1.98	0.3489	3.52	0.0521	4.12	309	6	304	9	290	94
Braga	LD-18	oc20j13	0.0491	2.26	0.3595	4.08	0.0533	4.00	309	7	312	11	338	92
Braga	LD-18	oc20g05	0.0495	2.12	0.3585	5.18	0.0512	6.42	312	6	311	14	248	146
Braga	LD-18	oc20h09	0.0496	3.32	0.3602	5.14	0.0527	3.82	312	10	312	14	316	88
											Concordia Age: 305.7 ± 1.9 Ma			
N40°34′09.3″	W007°15′03.7″													
Guarda	LD-19	oc21c05	0.0471	1.34	0.3350	3.02	0.0520	2.94	297	4	293	8	284	68
Guarda	LD-19	oc21c07	0.0472	1.76	0.3448	6.42	0.0540	6.00	297	5	301	17	368	136
Guarda	LD-19	oc21b10	0.0473	1.62	0.3418	2.42	0.0532	2.64	298	5	299	6	336	60
Guarda	LD-19	oc21b11	0.0474	1.69	0.3380	2.07	0.0530	1.56	298	3	294	4	328	36
Guarda	LD-19	oc21a05	0.0475	1.68	0.3384	2.66	0.0520	1.86	299	4	296	6	284	42
Guarda	LD-19	oc21c12	0.0476	1.70	0.3515	3.16	0.0538	3.14	300	5	307	8	362	70
Guarda	LD-19	oc21b14	0.0479	1.42	0.3568	5.43	0.0543	5.34	302	4	312	14	382	120
Guarda	LD-19	oc21c11	0.0480	1.54	0.3614	4.70	0.0540	2.42	302	5	313	6	368	54
											Concordia Age: 298.9 ± 1.6 Ma			
N40°33′49.1″	W005°26′13.1″													
El Alamo	LD-20	oc21d14	0.0477	2.68	0.3481	3.24	0.0528	4.24	301	8	303	9	320	96
El Alamo	LD-20	oc21d05	0.0483	2.48	0.3634	4.40	0.0549	3.06	304	5	315	8	408	68
El Alamo	LD-20	oc21d06	0.0482	2.58	0.3604	2.90	0.0539	2.82	304	8	313	8	368	64

Table 1. (continued)

Pluton	Sample	Analysis Number	Isotopic Ratios and 2σ (%) Errors						Ages and 2σ Absolute Errors (Ma)					
			$^{206}Pb/^{238}U$	$\pm2\sigma$	$^{207}Pb/^{235}U$	$\pm2\sigma$	$^{207}Pb/^{206}Pb$	$\pm2\sigma$	$^{206}Pb/^{238}U$	$\pm2\sigma$	$^{207}Pb/^{235}U$	$\pm2\sigma$	$^{207}Pb/^{206}Pb$	$\pm2\sigma$
El Alamo	LD-20	oc21d11	0.0486	2.18	0.3497	6.60	0.0532	5.80	306	6	304	17	334	132
El Alamo	LD-20	oc21d09	0.0493	2.42	0.3501	2.96	0.0516	3.44	310	7	305	8	268	78
El Alamo	LD-20	oc21d10	0.0493	1.54	0.3484	4.12	0.0521	3.76	310	5	304	11	288	86
El Alamo	LD-20	oc21e08	0.0496	2.02	0.3625	2.81	0.0527	2.54	312	5	314	6	314	58
											Concordia Age: 307.6 ± 3.5 Ma			
N40°31′23.1″	W005°25′25.8″													
El Miron	LD-21	oc21h06	0.0475	1.76	0.3427	5.00	0.0520	4.12	299	5	299	13	282	94
El Miron	LD-21	oc21h08	0.0483	1.84	0.3456	5.22	0.0517	5.82	304	5	301	14	270	134
El Miron	LD-21	oc21g09	0.0484	1.70	0.3624	5.00	0.0533	4.08	305	5	314	13	338	92
El Miron	LD-21	oc21h09	0.0489	1.56	0.3498	4.38	0.0528	3.90	307	5	305	12	318	88
El Miron	LD-21	oc21h07	0.0490	1.74	0.3626	3.18	0.0535	2.94	308	5	314	9	350	66
El Miron	LD-21	oc21h10	0.0490	2.16	0.3707	6.24	0.0549	4.66	309	7	320	17	406	104
El Miron	LD-21	oc21g10	0.0496	1.74	0.3715	5.82	0.0537	5.08	312	5	321	16	360	116
El Miron	LD-21	oc21g16	0.0498	1.50	0.3594	2.86	0.0521	2.74	313	5	312	8	290	64
El Miron	LD-21	oc21h14	0.0498	1.88	0.3600	3.47	0.0523	2.86	313	6	315	9	298	66
											Concordia Age: 306.8 ± 2.9 Ma			

[a]Sample geographical coordinates are given for each pluton.

geochemical and isotopic features of the granitoids and mafic rocks are described elsewhere [*Fernández-Suárez et al.*, 2000, 2011, and references therein]. As additional information, Table 2 shows the zircon saturation temperatures ($^{Zr}T_{sat}$) for the granitoids calculated using the equation of *Watson and Harrison* [1983] where data are available. The $^{Zr}T_{sat}$ data are used to distinguish between *hot* ($^{Zr}T_{sat} > 800°C$) and *cold* ($^{Zr}T_{sat} < 800°C$) granitoids [*Miller et al.*, 2003]. Hot granitoids have high whole-rock Zr content (usually >200 ppm) and low zircon inheritance (as deduced from cathodolumiscence imaging); cold granites have low whole-rock Zr content (usually <150 ppm) and high zircon inheritance (revealed by abundant cores in CL imaging or the presence of inherited lead components as indicated by highly discordant ID-TIMS analyses with $^{207}Pb/^{206}Pb$ ages much older than the crystallization age). In the case of the plutons

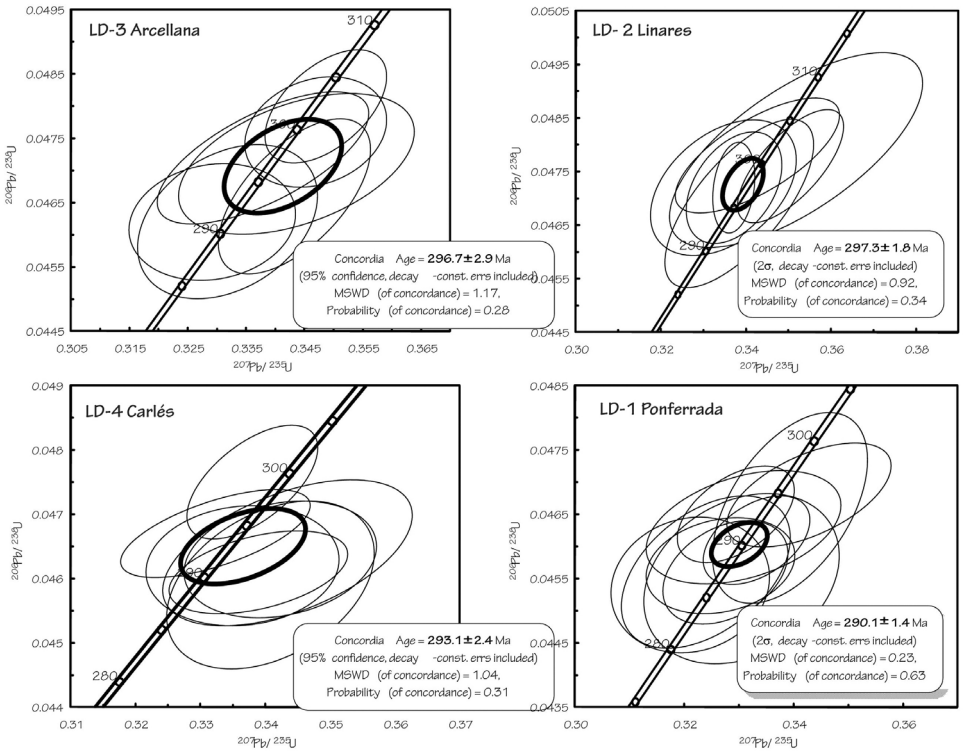

Figure 2. Concordia plots showing the U-Pb zircon age of the intrusions from the WALZ and CZ dated in this study.

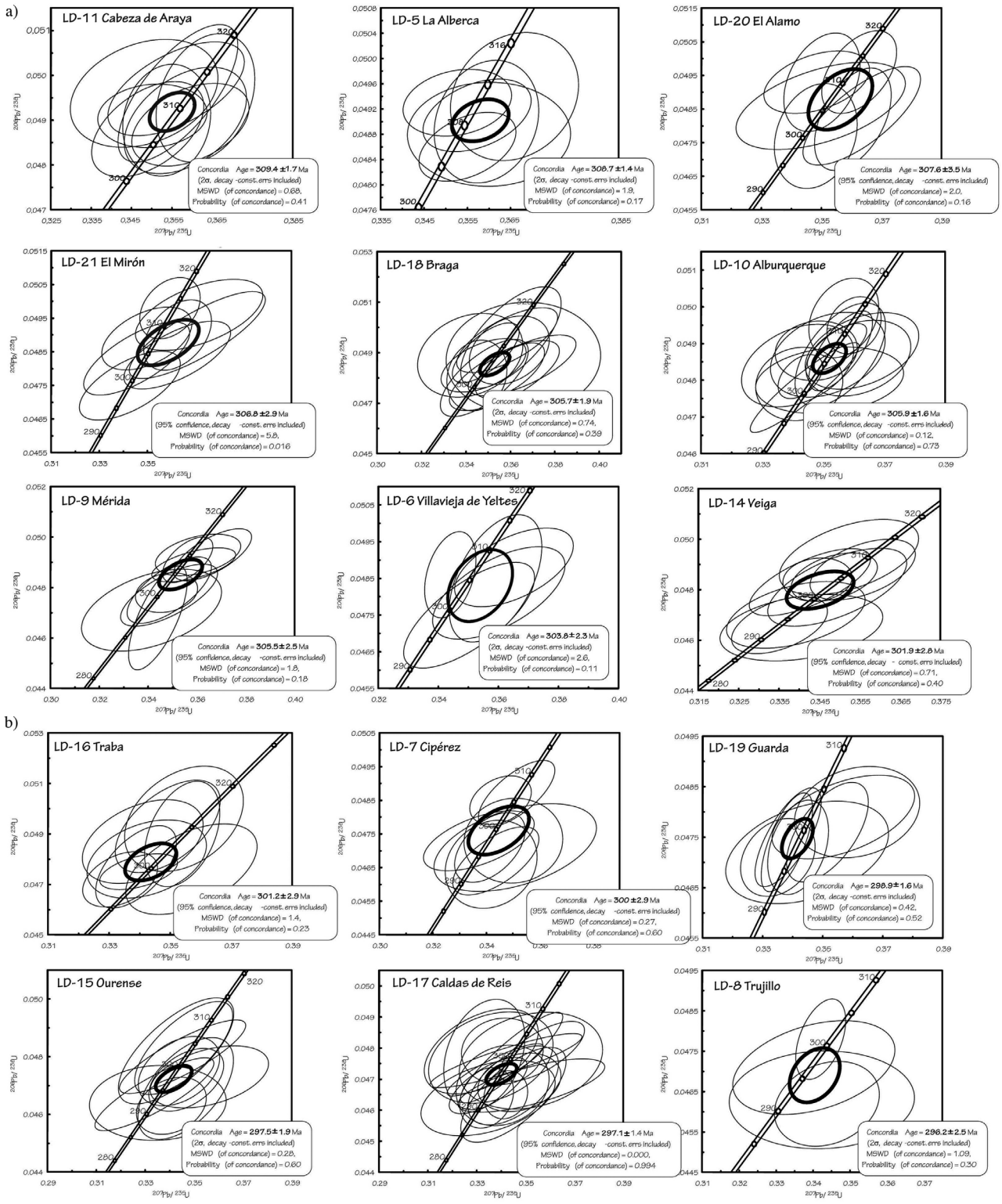

Figure 3. Concordia plots showing the U-Pb zircon age of the intrusions from the CIZ dated in this study.

Table 2. U-Pb Age Compilation Used in This Study

Pluton	Zone	Rock Type	U-Pb Age	2σ	T_{Zr} Sat[a] (°C)	Method	Source[b]
Cantabrian and Westasturian Leonese Zones							
San Ciprián	WALZ	Leucogranite	286	2	**717**	ID-TIMS	*Fernández-Suárez et al.* [2000]
Ancares	WALZ	Leucogranite	289	3	**703**	ID-TIMS	*Fernández-Suárez et al.* [2000]
Ponferrada	WALZ	Leucogranite	290	2	**713**	LAICPMS	
Boal	WALZ	Two-mica Monzogranite	291	3	**734**	ID-TIMS	*Fernández-Suárez et al.* [2000]
Peña prieta	CZ	Granodiorite	292	3	*800*	ID-TIMS	*Valverde-Vaquero et al.* [1999]
Carles	CZ	Granodiorite	293	2	*801*	LAICPMS	
El Courio	CZ	Q-monzodiorite	293	2	*822*	ID-TIMS	*Valverde-Vaquero et al.* [1999]
Vivero (Cortlandites)	WALZ	Hornblendite	293	3		ID-TIMS	*Fernández-Suárez et al.* [2000]
Porcia/Salave	WALZ	Quartz-Diorite	295	3	*806*	ID-TIMS	*Fernández-Suárez et al.* [2000]
Tojiza	WALZ	Granodiorite	295	2	*838*	ID-TIMS	*Fernández-Suárez et al.* [2000]
Linares	CZ	Granodiorite	297	2	*804*	LAICPMS	
Arcellana	CZ	Granodiorite	297	3	*801*	LAICPMS	
Arcellana	CZ	Granodiorite	297	6		ID-TIMS	*Valverde-Vaquero et al.* [1999]
Central Iberian Zone							
Gouveiras	CIZ	Leucogranite	289	3	**774**	U-Th-Pb in monazite (SHRIMP)	*Neiva et al.* [2009]
Paufito	CIZ	Leucogranite	290	3	**770**	ID-TIMS	*Dias et al.* [1998]
La Cabrera	CIZ	Two-mica Monzogranite	292	3	**785**	ID-TIMS	*Valverde-Vaquero* [1997]
Trujillo	CIZ	Leucogranite	296	3	**725**	LAICPMS	
Geres	CIZ	Leucogranite	296	2	**755**	ID-TIMS	*Dias et al.* [1998]
Caldas de Reis	CIZ	Granodiorite	297	2	*859*	LAICPMS	
Ourense	CIZ	Leucogranite	298	2	**771**	LAICPMS	
Guarda	CIZ	Two-mica Monzogranite	299	2	*808*	LAICPMS	
Vila Pouca de Aguiar	CIZ	Biot Monzogranite	299	3	**750**	ID-TIMS	*Martins et al.* [2009]
Ciperez	CIZ	Two-mica Monzogranite	300	3	*800*	LAICPMS	
Briteiros	CIZ	Two-mica Monzogranite	300	1		ID-TIMS	*Dias et al.* [1998]
Traba	CIZ	Leucogranite	301	3	**762**	LAICPMS	
Gouveiras	CIZ	Two-mica Monzogranite	302	3	**783**	U-Th-Pb in monazite (SHRIMP)	*Neiva et al.* [2009]
Veiga	CIZ	Two-mica Monzogranite	302	3	**774**	LAICPMS	
Villavieja de Yeltes	CIZ	Leucogranite	304	2	**764**	LAICPMS	
Cerro Mogabar	CIZ	Leucogranite	304	2		ID-TIMS	*Carracedo et al.* [2009]
Merida	CIZ	Leucogranite	306	3	**787**	LAICPMS	
Nisa-Albuquerque	CIZ	Two-mica Monzogranite	306	2	**760**	LAICPMS	
Nisa-Albuquerque	CIZ	Tonalite	307	2		SHRIMP II	*Solá et al.* [2009]
Braga	CIZ	Granodiorite	306	2	*843*	LAICPMS	
Navahermosa	CIZ	Gabbro	306	2		Cameca IMS270	*Zeck et al.* [2007]
Cota-Viseu	CIZ	Bt-monzogranite	306	5	*820*	ID-TIMS	*Valle Aguado et al.* [2005]
Celeiros	CIZ	Two mica Monzgranites	306	2		ID-TIMS	*Dias et al.* [1998]
La Bastida	CIZ	Gabbro	306	2		Cameca IMS270	*Bea et al.* [2006]
El Miron	CIZ	Q-diorite	307	3	*809*	LAICPMS	
Ledrada-Colmenar	CIZ	Cord-Biotite Monzogranite	307	2		Cameca IMS270	*Zeck et al.* [2007]
Agrela	CIZ	Biotite Granodiorite	307	4	*847*	ID-TIMS	*Dias et al.* [1998]
Berlanga islands	CIZ	Biotite Monzogranite	307	1		ID-TIMS	*Valverde-Vaquero et al.* [2010]
Celorico de Basto	CIZ	Biotite Monzogranite	308	4	*814*	ID-TIMS	*Dias et al.* [2002]
El Alamo	CIZ	Gabbro	308	3		LAICPMS	
Junqueira	CIZ	Two-mica Monzogranite	308	1	*810*	ID-TIMS	*Valle Aguado et al.* [2005]
Los Pedroches	CIZ	Granodiorite Bt ± Amph	308	2	*815*	ID-TIMS	*Carracedo et al.* [2009]
Toledo	CIZ	Gabbro	308	2	*851*[c]	Cameca IMS270	*Bea et al.* [2006]
La Alberca	CIZ	Granodiorite	309	2	*817*	LAICPMS	
Cabeza de Araya	CIZ	Cord-Bt Granodiorite	309	2	*819*	LAICPMS	
Arges	CIZ	Tonalite	309	4	*853*	Cameca IMS270	*Bea et al.* [2006]
Castelo Branco	CIZ	Granodiorite Bt ± Amph	309	2	*827*	ID-TIMS	*Antunes et al.* [2010]
Guajaraz	CIZ	Gabbro	311	5		Cameca IMS270	*Bea et al.* [2006]

[a]Zircon saturation temperature calculated with the equation of *Watson and Harrison* [1983]. Bold numbers are cold; italic numbers are hot.
[b]Blank rows indicate this study.
[c]Ti-in-Zircon thermometry.

considered herein, hot granitoids correspond mostly to infracrustal I-type granodiorites-monzogranites [see also *Fernández-Suárez et al.*, 2011] whereas cold granitoids are mostly mid-crustal S-type two-mica monzogranites and leucogranites.

[25] The data compiled in Table 2 (including the 19 new analyses of Table 1) show the following features:

[26] Granitoids and mafic rocks in the foreland fold and thrust belt (CZ + WALZ) (Figures 1 and 2 and Tables 1 and 2) have ages that range from 286 Ma to 297 Ma with a weighted average of 293 ± 2 Ma. The youngest rocks in this data set are the 286 ± 3 Ma peraluminous leucogranites in the WALZ, which have low Zr content (<60 ppm), high zircon inheritance [*Fernández-Suárez et al.*, 2000] and low

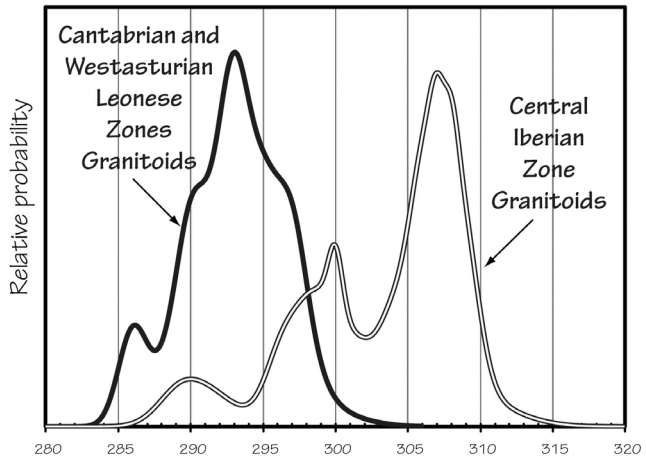

Figure 4. Probability density plot illustrating the age difference between intrusions in the WALZ + CZ and the in CIZ. The plot was constructed using the ages and errors reported in Table 2.

zircon saturation temperatures (ca. 700–720°C) typical of "cold" granites. Peraluminous leucogranites are absent in the Cantabrian Zone (the most external zone of the foreland fold and thrust belt) in which post-orogenic magmatism is dominated by mafic-intermediate rocks [*Corretgé et al.*, 2004].

[27] Granitoids and mafic rocks in the Central Iberian Zone (CIZ, Tables 1 and 2; Figures 1 and 3) display U-Pb ages that range from 311 ± 5 Ma to 289 ± 3 Ma with a weighted average of 304 ± 2 Ma. The probability density plot of Figure 4 shows the significant age difference between granitoids and mafic rocks in the CZ + WALZ with respect to those of the CIZ; this "age shift" is discussed below. Within the CIZ, mafic rocks (mainly gabbros, Table 2) have ages ranging from 311 ± 5 Ma to 306 ± 2 Ma with a weighted mean of 307 ± 1 Ma (MSWD = 1.2) which suggests a short duration for the pulse of mantle-derived magmatism in the CIZ, at least based on the exposed mafic rocks in the region. To our knowledge, no mafic rocks with ages younger than ca. 306 Ma have been identified in the CIZ. Mantle-derived mafic rocks in the CZ + WALZ are ca. 5 to 10 myr younger than their chemically and isotopically correlatives in the CIZ.

[28] The leucogranites and "cold" granitoids in the CIZ have ages younger than 306 Ma (weighted average of 299 ± 3 Ma) although "hot" granitoids also intrude after 306 Ma (e.g., Caldas de Reyes pluton, Table 2). Figure 5 illustrates the age shifts between mafic rocks + hot granitoids versus cold granitoids in both the CZ + WALZ and the CIZ. We consider these age differences to be relevant and their relevance is addressed in the discussion that follows.

5. Discussion

[29] Our U-Pb age data place constraints on models for the tectonic evolution of the NW Iberian Variscan belt in late-Carboniferous- early Permian times, and is used here to develop a time- and space- integrated hypothesis for the genesis of post-orogenic magmatism in this sector of the European Variscides.

[30] Post-orogenic magmatism in this realm of the Variscan orogen took place between ca. 310 and 285 Ma (i.e., Middle Pennsylvanian to Middle Cisuralian [*Gradstein et al.*, 2004]), representing a 25 myr time slice. The data confirm that these granitoid rocks were emplaced after the main episodes of collision-driven crustal thickening (initiated at ca. 360 Ma [*Dallmeyer et al.*, 1997]) and at least 15 Ma after the ensuing extensional collapse of the orogen (dated at ca. 330–320 Ma; [*Bea et al.*, 2006; *Valverde-Vaquero et al.*, 2006]). There is a significant difference in granitoid crystallization ages between the hinterland (CIZ) and the foreland fold and thrust belt (WALZ + CZ) (Figure 4).

[31] The data are also consistent with the hypothesis that the post-orogenic magmatism was coeval with the Late Pennsylvanian to Early Cisuralian development of an orocline that constitutes the Iberian-Armorican arc [*Weil et al.*, 2001, 2010]. Modeling of the IAA orocline as the result of bending of an initially linear orogen around a vertical axis shows that extension and lithospheric thinning is required in the outer arc of the orocline (CIZ) simultaneous with thickening and lithospheric root formation under the WALZ

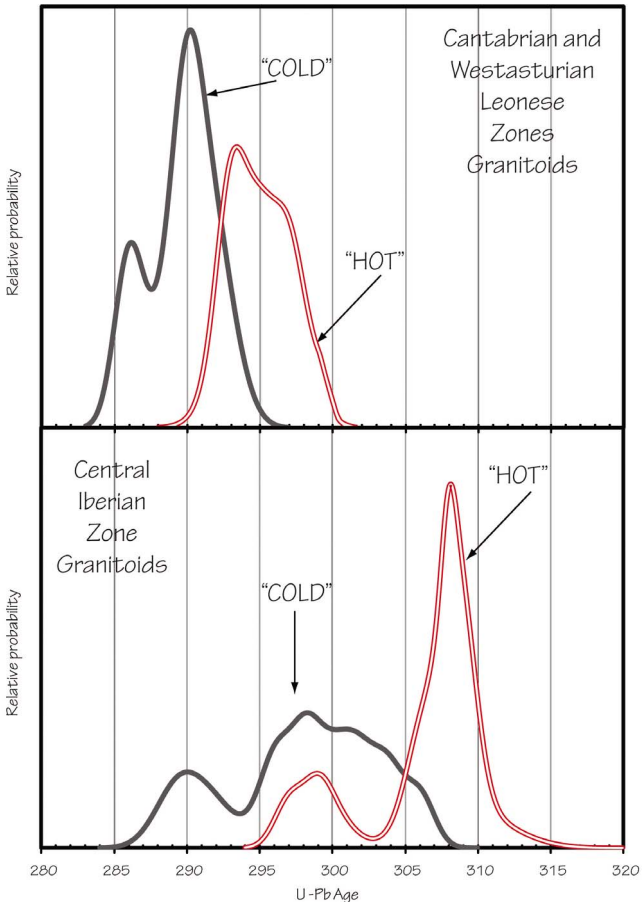

Figure 5. Probability density plot showing the age difference between hot granitoids + mafic rocks and cold granitoids in the WALZ + CZ and the in CIZ. The plot was constructed using the ages and errors reported in Table 2.

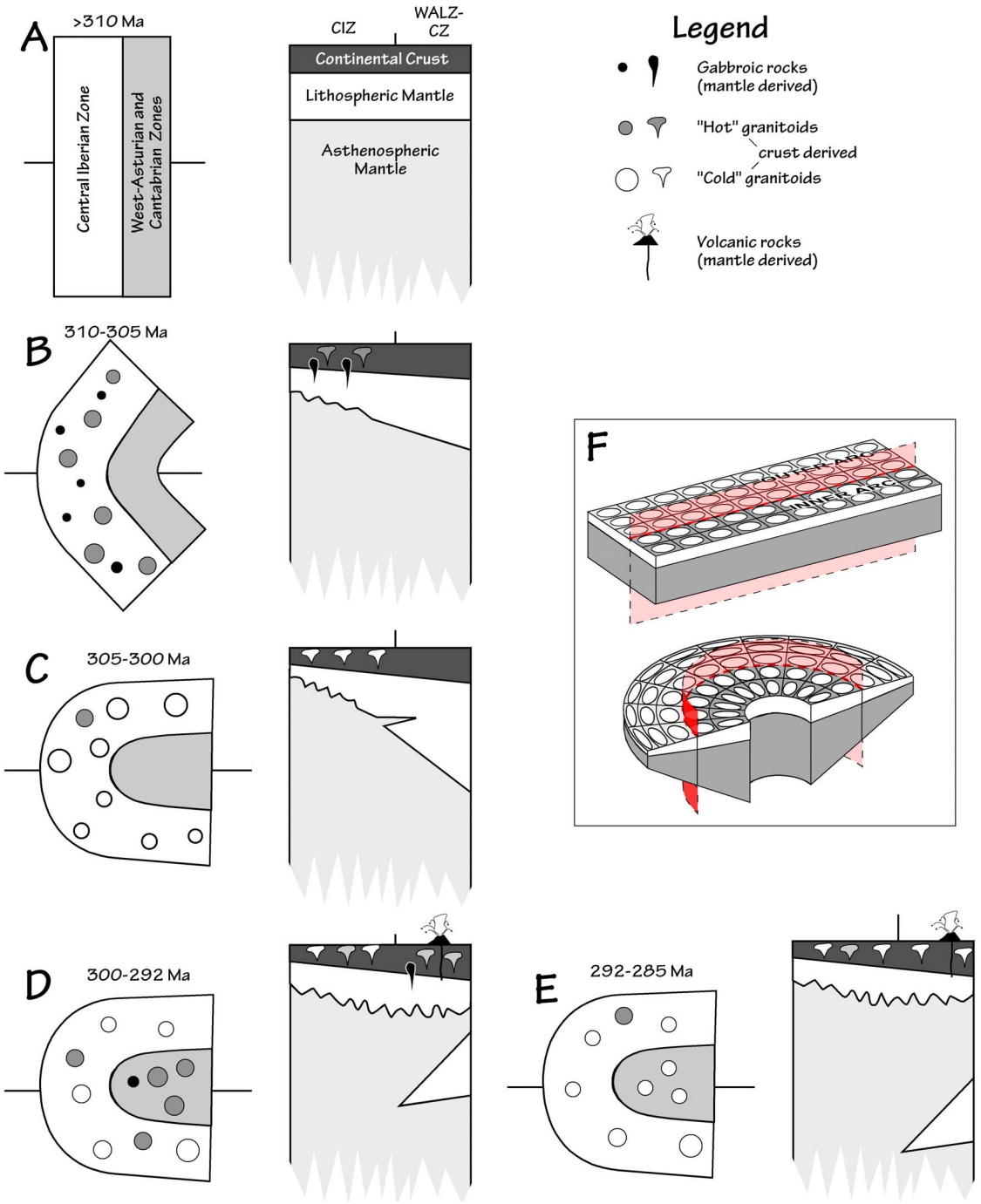

Figure 6. (a–e) Illustration showing the sequential development of the IAA and the genesis of post-orogenic granitoids and mafic rocks as a consecuence of lithospheric deformation caused by oroclinal development. See text for details. See also Animation S1 in the auxiliary material. (f) Depicts a conceptual 3D model of oroclinal buckling around a vertical axis by tangential longitudinal strain which explains the vertical lithospheric thickness variations from the outer to the inner arcs of the orocline (taken from *Gutiérrez-Alonso et al.* [2004]).

and CZ (inner arc) [*Gutiérrez-Alonso et al.*, 2004; *Weil et al.*, 2010] (Figure 6 and auxiliary material).[1]

[32] Post-tectonic Magmatism in the CIZ (hereafter termed the "outer arc" of the orocline (Figure 6 and auxiliary material) started at ca. 310 Ma with the intrusion of mantle-derived mafic rocks and "hot" granodiorite-monzogranite (with minor tonalite) intrusions whose isotopic and geochemical features suggest genesis by melting of predominantly metaigneous protoliths in the lower crust [*Fernández-Suárez et al.*, 2011; *Villaseca et al.*, 2009]. The crystallization ages of these earliest post-orogenic intrusions

[1]Auxiliary materials are available in the HTML. doi:10.1029/2010TC002845.

overlap with ^{40}Ar-^{39}Ar age of fabrics from an orogen-scale sub-vertical shear zone system (ca. 307 Ma [*Valle Aguado et al.*, 2005; *Gutiérrez-Alonso et al.*, 2010; *Rodríguez et al.*, 2003]). We speculate that these steep shear zones may have acted as structural conduits for the ascent of these early post-orogenic mantle-derived mafic melts and lower crustal granitoid melts. This early stage, that lasted for about 5 myr (310–305 Ma) (Figure 6a), was limited to the outer arc and involved little or no generation of peraluminous S-type leucogranites or two-mica monzogranites (cold granitoids).

[33] However, it should be mentioned that peraluminous Bt-Crd granodiorites and monzogranites in the CIZ (e.g., Cabeza de Araya and Ledrada-Colmenar plutons in Table 2) [*Capdevila et al.*, 1973; *Garcia-Moreno et al.*, 2007] did crystallize mainly within this early age interval (310–305 Ma). This observation is consistent with hypotheses that link the genesis of this particular type of more mafic peraluminous granitoid with the participation of mafic magmas at lower crustal levels [*Barbarin*, 1996]. S-type, two-mica peraluminous monzogranites and leucogranites in the CIZ have crystallization ages that peak at ca. 299 Ma, suggesting a "delay" in their genesis with respect to more mafic, deeper and hotter granitoids and mantle-derived mafic rocks (Figure 5). This ca 4–5 myr delay could be taken as the upwards travel time of the thermal anomaly that produced the melting of lithospheric mantle and lower crust. Nevertheless, hot granitoids continued to be produced during this younger time slice (e.g., Caldas de Reyes, Table 2) but no mafic mantle-derived mafic rocks younger than 306 Ma have been reported in the CIZ.

[34] Mantle and lower crustal melting peaked between ca 310 and 305 Ma, and middle crustal melting peaked at ca 300 Ma in the CIZ. We interpret these observations to reflect lithospheric thinning in the outer arc of the orocline (Figure 6) that facilitated asthenospheric mantle upwelling and concomitant melting of the thinned lithospheric mantle and the lower crust [*Gutiérrez-Alonso et al.*, 2004; *Weil et al.*, 2010] giving rise to the oldest mafic rocks and "hot" granitoids of the CIZ. This upward-migrating thermal anomaly reached mid-crustal levels ca. 5 myr later, causing middle crustal melting and genesis of typical two-mica, cold, peraluminous leucogranites and monzogranites [*Barbarin*, 1996; *Sylvester*, 1998]. At this stage, lower crustal melting was still happening but mantle melting either ceased (there are no gabbros younger than 306 in the CIZ) or melts could no longer transect the mantle-crust interface.

[35] U-Pb dating of zircon from lower crustal granulite xenoliths from the CIZ entrained in Middle Permian dykes [*Fernández-Suárez et al.*, 2006; *Villaseca et al.*, 1999] yield ages between ca 308 and 280 Ma (weighted mean 295 Ma) indicating extensive granulitization of the lower crust coeval with the post-orogenic magmatism in the CIZ.

[36] In the foreland fold and thrust belt (CZ + WALZ, inner arc of the orocline) there is no record of igneous activity prior to 297 Ma (Figure 6 and auxiliary material) and the oldest rocks are mantle-derived gabbros and quartz-diorites (Table 2). Intrusion of mafic rocks and "hot" I-type granitoids of lower crustal origin took place between 297 and 292 Ma indicating that melting of the inner arc lithospheric mantle-lower crust ensemble was initiated ca. 10–12 myr after it started under the CIZ (outer arc) (Figure 4). This delay can be explained considering that during formation of the IAA, lithospheric extension and melting in the outer arc (CIZ) was coeval with lithospheric root formation in the inner arc of the orocline [*Gutiérrez-Alonso et al.*, 2004; *Weil et al.*, 2010] (see Figure 6f for a 3D representation of oroclinal buckling around a vertical axis by tangential longitudinal strain). We suggest that the age of the oldest mantle-derived mafic rocks in the CZ (ca. 297 Ma) mark the detachment of the lithospheric root that developed beneath the inner arc during orocline formation, and that concomitant upwelling of asthenospheric mantle then triggered mantle-lower crustal melting under the inner arc. Progressive foundering of the lithospheric root and continued asthenospheric upwelling maintained the conditions for melting during the subsequent ca 10–12 myr. As in the case of the CIZ, peraluminous leucogranites and cold granitoids in the inner arc (ca. 292–286 Ma) are younger than the mafic rocks and hot granitoids (Figure 5). These magmas were generated by melting of mid-crustal metasedimentary protoliths [*Fernández-Suárez et al.*, 2000; *Fernández-Suárez*, 1994] upon upwards migration of the thermal anomaly created at the crust-mantle interface by foundering of the lithospheric root. In the inner arc, the apparent age difference between the oldest mantle-derived rocks and the oldest mid-crustal peraluminous leucogranites is ca 8 myr, similar to the equivalent delay in the CIZ (Figure 5 and Table 2). S-type peraluminous monzogranites and leucogranites are virtually absent in the CZ and relatively abundant in the more internal WALZ (Figure 1). The WALZ is transitional with the hinterland and does contain a fertile, shale and greywacke-rich middle-crust capable of producing peraluminous monzogranite-leucogranite melts at low temperatures (e.g., Ancares, Ponferrada, San Ciprian intrusions, Table 2 [*Fernández-Suárez*, 1994]). On the other hand, the thinner and more brittle crust in the CZ, lacking a fertile mid-crust, was readily fractured during the IAA genesis, facilitating ascent of mantle-derived mafic rocks.

[37] The intrusion ages of post-orogenic granitoids in the W-Iberian Variscan belt fit the model of orocline-driven lithospheric-thinning/delamination as a heat engine for the voluminous magmatic event that took place across the entire orogenic belt from ca. 310 to 285 Ma. The aforementioned alternative hypotheses, namely radiogenic heat production in a thickened crust [*Bea et al.*, 2003] or the presence of an ephemeral mantle plume [*Pinarelli and Rottura*, 1995] seem less likely. The former hypothesis does not fit the chronology of post-orogenic magmatism, which peaked ca. 20 to 30 myr after the extensional collapse of the orogenic belt. Furthermore, late-Variscan extension (Late Pennsylvanian-Early Permian) was minor and is considered to have been insufficient to cause by itself the voluminous post-orogenic magmatism [*Doblas et al.*, 1994; *Ziegler and Dèzes*, 2006]. With regard to the latter hypothesis, if a plume was responsible for post-orogenic magmatism, it would have needed to be located beneath Iberia from ca. 310 to 285 Ma. However, Iberia moved northward between 10° and 40° latitude between 340 and 285 Ma [*Cocks and Torsvik*, 2006; *Stampfli and Borel*, 2002] and consequently a plume should have generated a >2000 km long N-S magmatic track. Such

a track is not observed and the spatial distribution of post-orogenic magmatism is not consistent with its presence under Iberia.

6. Conclusions

[38] U-Pb dating of a significant number of post-orogenic intrusions across the orogenic belt offers support for the models of *Gutiérrez-Alonso et al.* [2004, 2011] and *Weil et al.* [2010] that link post-orogenic magmatism with orocline-driven lithospheric thinning/delamination and explains the 25 myr of post-orogenic magmatism. The temporal and spatial relationship between orocline development and late-Variscan magmatism is depicted in Figure 6 and in Animation S1 in the auxiliary material and can be summarized as follows:

[39] 1) ca. 310–305 Ma (Figures 6a and 6b): Oroclinal bending starts, producing lithospheric thinning and asthenospheric upwelling in the outer arc (CIZ) and concomitant melting of the lithospheric mantle-lower crust ensemble. Mafic rocks, infracrustal (hot) I-type granitoids and peraluminous Bt-Crd granodiorites and monzogranites are produced in this early episode. A coeval network of shear zones may have acted as the structural conduits for the ascent of these magmas. In this time interval, a lithospheric root was created under the inner arc but no magmas were generated.

[40] 2) ca. 305–300 (Figure 6c). Melting continues under the CIZ producing more lower crustal (hot) granitoids and mid-crustal melting is initiated, generating peraluminous (cold) two-mica leucogranites and monzogranites. Mantle melts are no longer being generated or are arrested at the base of the crust. During this interval, the lithospheric root under the WALZ + CZ zones (inner arc of the orocline) grew owing to progressive arc closure and concomitant tightening in the core of the orocline. The root probably became unstable and started to detach from the upper part of the mantle lithosphere.

[41] 3) ca. 300–292 (Figure 6d). At ca. 297 Ma melting in the lithospheric mantle and the lower crust is initiated under the inner arc (WALZ + CZ) by upwelling of asthenospheric mantle that replaced the foundering lithospheric root ca. 12 myr after the initiation of oroclinal bending. During this interval, melting continued in lower crustal and mid-crustal levels of the CIZ.

[42] 4) ca. 292–285 Ma (Figure 6e): The lithosphere cools down progressively and there is a drastic attenuation of lower crustal high-temperature melts and mostly cold granitoids and leucogranites are produced by low temperature (ca. <800°C) melting in mid-crustal sections. By ca. 285 Ma, the thermal engine generated by orocline-driven lithospheric thinning/delamination had cooled down beyond its capability to produce significant amounts of mantle or crustal melts. This final scenario is in agreement with temperature calculations based on the Ti-in-Zircon and Zr-in-Rutile thermometers applied to those minerals on lower crustal granulite xenoliths under the CIZ (entrained in late Permian alkaline magmas) which indicate significant cooling of the lower crust between ca 285 and 280 Ma [*Orejana et al.*, 2011].

[43] This model should be further tested in the northern branch of the IAA outcropping in Ireland, Great Britain and France where more U-Pb ages of post-tectonic granitoid bodies are needed in order to establish a pattern hypothetically consistent with the one proposed herein.

[44] In summary, orocline formation and post-orogenic magmatism in the Variscan orogen are very probably genetically related. Lithospheric thinning around the outer margin of the developing arc facilitated asthenospheric upwelling and initiated mantle melting and subsequent crustal melting. Magmatism swept toward the core of the arc as the thickened lithospheric root that would have developed beneath the inner arc of the orocline detached and foundered. Oroclines and similar post-orogenic granitoids are common constituents of numerous orogenic belts [*Johnston*, 2008; *Johnston and Gutiérrez-Alonso*, 2010] and they may well be similarly related elsewhere.

[45] The above scenario fits the time-frame proposed for the detachment of a lithospheric mantle root, which is thought to occur in a relatively short time (5–10 Ma [*Schott and Schmeling*, 1998]). In addition, our hypothesis is in agreement with models derived from geophysical evidence in present-day cases of lithospheric root detachment and foundering, e.g., the Vrancea region of the Carpathians [*Fillerup et al.*, 2010].

[46] **Acknowledgments.** G.G.-A., D.P.-G., M.P.F., and J.C.G.'s financial support was supplied by Research Projects ODRE and ODRE II ("Oroclines and Delamination: Relations and Effects") CGL2006-00902 and CGL2009-1367 from the Spanish Ministry of Science and Innovation. NSERC Canada is thanked for its continuing support through Discovery (S.T.J. and J.B.M.) and Research Capacity Development (J.B.M.) grants. J.F.S. wishes to acknowledge financial support from project CONSOLIDER CGL2007-65338-C02-01/BTE by the Spanish Ministry of Science and Technology. This is a contribution to IGCP 574.

References

Abrajevitch, A., R. Van der Voo, M. L. Bazhenov, N. M. Levashova, and P. J. A. McCausland (2008), The role of the Kazakhstan orocline in the late Paleozoic amalgamation of Eurasia, *Tectonophysics*, *455*(1–4), 61–76, doi:10.1016/j.tecto.2008.05.006.

Allmendinger, R. W., R. Smalley, M. Bevis, H. Caprio, and B. Brooks (2005), Bending the Bolivian orocline in real time, *Geology*, *33*(11), 905–908, doi:10.1130/G21779.1.

Alonso, J. L., A. Marcos, and A. Suarez (2009), Paleogeographic inversion resulting from large out of sequence breaching thrusts: The Leon Fault (Cantabrian Zone, NW Iberia). A new picture of the external Variscan Thrust Belt in the Ibero-Armorican Arc, *Geol. Acta*, *7*(4), 451–473.

Antunes, I. M. H. R., A. M. R. Neiva, and M. M. V. G. Silva (2010), Isotopic geochronology of granitic rocks from the Central Iberian Zone: Comparison of methodologies, *Estud. Geol.*, *66*(1), 45–50, doi:10.3989/egeol.40143.097.

Aranguren, A., J. Cuevas, J. M. Tubia, T. Roman-Berdiel, A. Casas-Sainz, and A. Casas-Ponsati (2003), Granite laccolith emplacement in the Iberian arc: AMS and gravity study of the La Tojiza pluton (NW Spain), *J. Geol. Soc.*, *160*, 435–445, doi:10.1144/0016-764902-079.

Arenas, R., and J. R. M. Catalan (2003), Low-P metamorphism following a Barrovian-type evolution. Complex tectonic controls for a common transition, as deduced in the Mondonedo thrust sheet (NW Iberian-Massif), *Tectonophysics*, *365*(1–4), 143–164, doi:10.1016/S0040-1951(03)00020-9.

Arenas, R., J. R. M. Catalan, S. S. Martinez, J. Fernández-Suárez, P. Andonaegui, J. A. Pearce, and F. Corfu (2007), The Vila de Cruces ophiolite: A remnant of the early Rheic Ocean in the Variscan suture of Galicia (northwest Iberian Massif), *J. Geol.*, *115*(2), 129–148, doi:10.1086/510645.

Barbarin, B. (1996), Genesis of the two main types of peraluminous granitoids, *Geology*, *24*(4), 295–298, doi:10.1130/0091-7613(1996)024<0295:GOTTMT>2.3.CO;2.

Barbarin, B. (1999), A review of the relationships between granitoid types, their origins and their geodynamic environments, *Lithos*, *46*(3), 605–626, doi:10.1016/S0024-4937(98)00085-1.

Bastida, F., J. Aller, J. A. Pulgar, N. C. Toimil, F. J. Fernandez, N. C. Bobillo-Ares, and C. O. Menendez (2010), Folding in orogens: A case study in the northern Iberian Variscan Belt, *Geol. J.*, *45*(5–6), 597–622, doi:10.1002/gj.1199.

Bea, F., P. Montero, and T. Zinger (2003), The nature, origin, and thermal influence of the granite source layer of Central Iberia, *J. Geol.*, *111*(5), 579–595, doi:10.1086/376767.

Bea, F., P. G. Montero, F. Gonzalez-Lodeiro, C. Talavera, J. F. Molina, J. H. Scarrow, M. J. Whitehouse, and T. Zinger (2006), Zircon thermometry and U-Pb ion-microprobe dating of the gabbros and associated migmatites of the Variscan Toledo Anatectic Complex, Central Iberia, *J. Geol. Soc.*, *163*, 847–855, doi:10.1144/0016-76492005-143.

Beccaluva, L., A. Azzouni-Sekkal, A. Benhallou, G. Bianchini, R. M. Ellam, M. Marzola, F. Siena, and F. M. Stuart (2007), Intracratonic asthenosphere upwelling and lithosphere rejuvenation beneath the Hoggar swell (Algeria): Evidence from HIMU metasomatised lherzolite mantle xenoliths, *Earth Planet. Sci. Lett.*, *260*(3–4), 482–494, doi:10.1016/j.epsl.2007.05.047.

Bonin, B. (2004), Do coeval mafic and felsic magmas in post-collisional to within-plate regimes necessarily imply two contrasting, mantle and crustal, sources? A review, *Lithos*, *78*(1–2), 1–24, doi:10.1016/j.lithos.2004.04.042.

Caldwell, W. B., S. L. Klemperer, S. S. Rai, and J. F. Lawrence (2009), Partial melt in the upper-middle crust of the northwest Himalaya revealed by Rayleigh wave dispersion, *Tectonophysics*, *477*(1–2), 58–65, doi:10.1016/j.tecto.2009.01.013.

Capdevila, R., L. G. Corretge, and P. Floor (1973), Les granitoides varisques de la Meseta Iberique, *Bull. Soc. Geol. Fr.*, *15*, 209–228.

Carracedo, M., J. L. Paquette, A. Alonso Olazabal, J. F. Santos Zalduegui, S. García de Medinabeitia, M. Tiepolo, and J. I. Gil Ibarguchi (2009), U–Pb dating of granodiorite and granite units of the Los Pedroches batholith. Implications for geodynamic models of the southern Central Iberian Zone (Iberian Massif), *Int. J. Earth Sci.*, *98*(7), 1609–1624, doi:10.1007/s00531-008-0317-0.

Castiñeiras, P., C. Villaseca, L. Barbero, and C. M. Romera (2008), SHRIMP U-Pb zircon dating of anatexis in high-grade migmatite complexes of Central Spain: Implications in the Hercynian evolution of Central Iberia, *Int. J. Earth Sci.*, *97*, 35–50, doi:10.1007/s00531-006-0167-6.

Cocks, L. R. M., and T. H. Torsvik (2006), European geography in a global context from the Vendian to the end of the Palaeozoic, in *European Lithosphere Dynamics*, edited by D. G. Gee and R. A. Stephenson, pp. 83–95, Geol. Soc., London.

Corretgé, L. G., O. Suárez, G. Galán, and J. Fernández-Suárez (2004), Magmatismo, in *Geología de España*, edited by J. A. Vera, pp. 63–68, SGE-IGME, Madrid.

Dallmeyer, R. D., and J. I. G. Ibarguchi (1990), Age of amphibolitic metamorphism in the ophiolitic unit of the Morais allochthon (Portugal): Implications for early hercynian orogenesis in the Iberian Massif, *J. Geol. Soc.*, *147*, 873–878, doi:10.1144/gsjgs.147.5.0873.

Dallmeyer, R. D., J. R. M. Catalan, R. Arenas, J. I. G. Ibarguchi, G. G. Alonso, P. Farias, F. Bastida, and J. Aller (1997), Diachronous Variscan tectonothermal activity in the NW Iberian Massif: Evidence from $^{40}Ar/^{39}Ar$ dating of regional fabrics, *Tectonophysics*, *277*(4), 307–337, doi:10.1016/S0040-1951(97)00035-8.

Davies, J. H., and F. Von Blanckenburg (1995), Slab breakoff: A model of lithosphere detachment and its test in the magmatism and deformation of collisional orogens, *Earth Planet. Sci. Lett.*, *129*(1–4), 85–102, doi:10.1016/0012-821X(94)00237-S.

Depine, G. V., C. L. Andronicos, and J. Phipps-Morgan (2008), Near-isothermal conditions in the middle and lower crust induced by melt migration, *Nature*, *452*(7183), 80–83, doi:10.1038/nature06689.

Dias, G., J. Leterrier, A. Mendes, P. P. Simoes, and J. M. Bertrand (1998), U-Pb zircon and monazite geochronology of post-collisional Hercynian granitoids from the Central Iberian Zone (Northern Portugal), *Lithos*, *45*(1–4), 349–369, doi:10.1016/S0024-4937(98)00039-5.

Dias, G., P. P. Simoes, N. Ferreira, and J. Leterrier (2002), Mantle and crustal sources in the genesis of late-Hercynian granitoids (NW Portugal): Geochemical and Sr-Nd isotopic constraints, *Gondwana Res.*, *5*(2), 287–305, doi:10.1016/S1342-937X(05)70724-3.

Diez Balda, M. A., J. R. Martínez Catalán, and P. Ayarza Arribas (1995), Syn-collisional extensional collapse parallel to the orogenic trend in a domain of steep tectonics: The Salamanca Detachment Zone (Central Iberian Zone, Spain), *J. Struct. Geol.*, *17*(2), 163–182, doi:10.1016/0191-8141(94)E0042-W.

Doblas, M., et al. (1994), Extensional tectonics in the central Iberian Peninsula during the Variscan to Alpine transition, *Tectonophysics*, *238*(1–4), 95–116, doi:10.1016/0040-1951(94)90051-5.

Fernández-Suárez, J. (1994), Petrología de los granitos peralumínicos y metamorfismo de la banda Boal-Los Ancares, Ph.D. dissertation, Univ. de Oviedo, Oviedo, Spain.

Fernández-Suárez, J., G. Gutierrez-Alonso, G. A. Jenner, and S. E. Jackson (1998), Geochronology and geochemistry of the Pola de Allande granitoids (northern Spain): Their bearing on the Cadomian-Avalonian evolution of northwest Iberia, *Can. J. Earth Sci.*, *35*, 1439–1453, doi:10.1139/e98-074.

Fernández-Suárez, J., G. R. Dunning, G. A. Jenner, and G. Gutiérrez-Alonso (2000), Variscan collisional magmatism and deformation in NW Iberia: Constraints from U-Pb geochronology of granitoids, *J. Geol. Soc.*, *157*, 565–576, doi:10.1144/jgs.157.3.565.

Fernández-Suárez, J., G. G. Alonso, and T. E. Jeffries (2002), The importance of along-margin terrane transport in northern Gondwana: Insights from detrital zircon parentage in Neoproterozoic rocks from Iberia and Brittany, *Earth Planet. Sci. Lett.*, *204*(1–2), 75–88, doi:10.1016/S0012-821X(02)00963-9.

Fernández-Suárez, J., R. Arenas, T. E. Jeffries, M. J. Whitehouse, and C. Villaseca (2006), A U-Pb study of zircons from a lower crustal granulite xenolith of the Spanish central system: A record of Iberian lithospheric evolution from the Neoproterozoic to the Triassic, *J. Geol.*, *114*(4), 471–483, doi:10.1086/504180.

Fernández-Suárez, J., R. Arenas, J. Abati, J. R. M. Catalan, M. J. Whitehouse, and T. E. Jeffries (2007), U-Pb chronometry of polymetamorphic high-pressure granulites: An example from the allochthonous terranes of the NW Iberian Variscan belt, in *4-D Framework of Continental Crust*, edited by R. D. Hatcher Jr. et al., *GSA Mem.*, *200*, 469–488.

Fernández-Suárez, J., G. Gutiérrez-Alonso, S. T. Johnston, T. E. Jeffries, D. Pastor-Galan, G. A. Jenner, and J. B. Murphy (2011), Iberian late-Variscan granitoids: Some considerations on crustal sources and the significance of "mantle extraction ages," *Lithos*, *123*, 121–132, doi:10.1016/j.lithos.2010.09.010.

Fillerup, M. A., J. H. Knapp, C. C. Knapp, and V. Raileanu (2010), Mantle earthquakes in the absence of subduction? Continental delamination in the Romanian Carpathians, *Lithosphere*, *2*(5), 333–340, doi:10.1130/L102.1.

Garcia-Moreno, O., L. G. Corretge, and A. Castro (2007), Processes of assimilation in the genesis of cordierite leucomonzogranites from the Iberian massif: A short review, *Can. Mineral.*, *45*, 71–85, doi:10.2113/gscanmin.45.1.71.

Gómez Barreiro, J. G., J. R. Wijbrans, P. Castiñeiras, J. R. M. Catalán, R. Arenas, F. D. Garcia, and J. Abati (2006), $^{40}Ar/^{39}Ar$ laserprobe dating of mylonitic fabrics in a polyorogenic terrane of NW Iberia, *J. Geol. Soc.*, *163*, 61–73, doi:10.1144/0016-764905-012.

Gradstein, F. M., J. G. Ogg, and A. G. Smith (2004), *A Geologic Time Scale 2004*, Cambridge Univ. Press, Cambridge, U. K.

Gutiérrez-Alonso, G., J. Fernández-Suárez, and A. B. Weil (2004), Orocline triggered lithospheric delamination, in *Paleomagnetic and Structural Analysis of Orogenic Curvature*, edited by A. B. Weil and A. Sussman, *Spec. Pap. Geol. Soc. Am.*, *383*, 121–130, doi:10.1130/0-8137-2383-3(2004)383[121:OTLD]2.0.CO;2.

Gutiérrez-Alonso, G., J. Fernández-Suárez, A. S. Collins, I. Abad, and F. Nieto (2005), Amazonian mesoproterozoic basement in the core of the Ibero-Armorican Arc: $^{40}Ar/^{39}Ar$ detrital mica ages complement the zircon's tale, *Geology*, *33*(8), 637–640, doi:10.1130/G21485.1.

Gutiérrez-Alonso, G., J. B. Murphy, J. Fernández-Suárez, and M. A. Hamilton (2008a), Rifting along the northern Gondwana margin and the evolution of the Rheic Ocean: A Devonian age for the El Castillo volcanic rocks (Salamanca, Central Iberian Zone), *Tectonophysics*, *461*(1–4), 157–165, doi:10.1016/j.tecto.2008.01.013.

Gutiérrez-Alonso, G., J. Fernández-Suárez, A. B. Weil, J. B. Murphy, R. D. Nance, F. Corfu, and S. T. Johnston (2008b), Self-subduction of the Pangaean global plate, *Nat. Geosci.*, *1*(8), 549–553, doi:10.1038/ngeo250.

Gutiérrez-Alonso, G., J. Fernández-Suárez, T. E. Jeffries, A. S. Collins, S. T. Johnston, E. Gonzalez-Clavijo, D. Pastor-Galan, and A. B. Weil (2010), Absolute age ($^{40}Ar^{*}$-^{39}Ar and U-Pb) constrains on oroclinedevelopment and related lithospheric delamination in the Iberian Armorican Arc, *e-Terra*, *23*(4). [Available at http://metododirecto.pt/CNG2010/index.php/vol/article/viewFile/486/454.]

Gutiérrez-Alonso, G., J. B. Murphy, J. Fernández-Suárez, A. B. Weil, M. P. Franco, and J. C. Gonzalo (2011), Lithospheric delamination in the core of Pangea: Sm-Nd insights from the Iberian mantle, *Geology*, *39*(2), 155–158, doi:10.1130/G31468.1.

Ibarguchi, J. I. G., M. Mendia, J. Girardeau, and J. J. Peucat (1990), Petrology of eclogites and clinopyroxene garnet metabasites from the Cabo-Ortegal Complex (northwestern Spain), *Lithos*, *25*(1–3), 133–162, doi:10.1016/0024-4937(90)90011-O.

Jeffries, T. E., J. Fernández-Suárez, F. Corfu, and G. G. Alonso (2003), Advances in U-Pb geochronology using a frequency quintupled Nd: YAG based laser ablation system (λ = 213 nm) and quadrupole based ICP-MS, *J. Anal. At. Spectrom.*, *18*(8), 847–855, doi:10.1039/b300929g.

Johnston, S. T. (2001), The Great Alaskan Terrane Wreck: Reconciliation of paleomagnetic and geological data in the northern Cordillera, *Earth Planet. Sci. Lett.*, *193*(3–4), 259–272, doi:10.1016/S0012-821X(01)00516-7.

Johnston, S. T. (2008), The Cordilleran ribbon continent of North America, *Annu. Rev. Earth Planet. Sci.*, *36*, 495–530, doi:10.1146/annurev.earth.36.031207.124331.

Johnston, S. T., and G. Gutiérrez-Alonso (2010), The North American Cordillera and West European Variscides: Contrasting interpretations of similar mountain systems, *Gondwana Res.*, *17*(2–3), 516–525, doi:10.1016/j.gr.2009.11.006.

Lago, M., E. Arranz, A. Pocovi, C. Gale, and A. Gil-Imaz (2004), Permian magmatism and basin dynamics in the southern Pyrenees: A record of the transition from late Variscan transtension to early Alpine extension, in *Permo-Carboniferous Magmatism and Rifting in Europe*, edited by M. Wilson et al., *Geol. Soc. Spec. Publ.*, *223*, 439–464, doi:10.1144/GSL.SP.2004.223.01.19.

Levashova, N. M., K. E. Degtyareva, M. L. Bazhenov, A. Q. Collins, and R. Van der Voo (2003), Middle paleozoic paleomagnetism of east Kazakhstan: Post-Middle Devonian rotations in a large-scale orocline in the central Ural-Mongol belt, *Tectonophysics*, *377*(3–4), 249–268, doi:10.1016/j.tecto.2003.09.013.

Ludwig, K. R. (1998), On the treatment of concordant uranium-lead ages, *Geochim. Cosmochim. Acta*, *62*(4), 665–676, doi:10.1016/S0016-7037(98)00059-3.

Ludwig, K. R. (2003), User's manual for Isoplot 3.00: A geochronological toolkit for Microsoft Excel, *Berkeley Geochronol. Cent. Spec. Publ. 4*, Berkeley Geochronol. Cent., Berkeley, Calif.

Martínez Catalán, J. R., R. Arenas, F. Díaz Garcia, and J. Abati (1997), Variscan accretionary complex of northwest Iberia: Terrane correlation and succession of tectonothermal events, *Geology*, *25*(12), 1103–1106, doi:10.1130/0091-7613(1997)025<1103:VACONI>2.3.CO;2.

Martínez Catalán, J. R., R. Arenas, and M. A. Díez Balda (2003), Large extensional structures developed during emplacement of a crystalline thrust sheet: The Mondonedo nappe (NW Spain), *J. Struct. Geol.*, *25*(11), 1815–1839, doi:10.1016/S0191-8141(03)00038-5.

Martínez Catalán, J. R., R. Arenas, F. D. Garcia, P. G. Cuadra, J. Gomez-Barreiro, J. Abati, P. Castiñeiras, J. Fernández-Suárez, S. S. Martinez, and P. Andonaegui (2007), Space and time in the tectonic evolution of the northwestern Iberian Massif: Implications for the Variscan belt, in *4-D Framework of Continental Crust*, edited by R. D. Hatcher Jr. et al., *GSA Mem.*, 200, 403–423.

Martínez Catalán, J. R., et al. (2009), A rootless suture and the loss of the roots of a mountain chain: The Variscan Belt of NW Iberia, *C. R. Geosci.*, *341*, 114–126.

Martins, H. C. B., H. Sant'Ovaia, and F. Noronha (2009), Genesis and emplacement of felsic Variscan plutons within a deep crustal lineation, the Penacova-Régua-Verín fault: An integrated geophysics and geochemical study (NW Iberian Peninsula), *Lithos*, *111*, 142–155, doi:10.1016/j.lithos.2008.10.018.

Mendía Aranguren, M. S. (2000), Petrología de la Unidad Eclogítica del Complejo de Cabo Ortegal (NW de España), Ph.D. dissertation, Lab. Xeolóxico de Laxe, Univ. da Coruña, La Coruña, Spain.

Miller, C. F., S. M. McDowell, and R. W. Mapes (2003), Hot and cold granites? Implications of zircon saturation temperatures and preservation of inheritance, *Geology*, *31*(6), 529–532, doi:10.1130/0091-7613(2003)031<0529:HACGIO>2.0.CO;2.

Miller, J. S., J. E. P. Matzel, C. F. Miller, S. D. Burgess, and R. B. Miller (2007), Zircon growth and recycling during the assembly of large, composite arc plutons, *J. Volcanol. Geotherm. Res.*, *167*(1–4), 282–299, doi:10.1016/j.jvolgeores.2007.04.019.

Montero, P., F. Bea, F. Gonzalez-Lodeiro, C. Talavera, and M. J. Whitehouse (2007), Zircon ages of the metavolcanic rocks and metagranites of the Ollo de Sapo Domain in central Spain: implications for the neoproterozoic to early palaeozoic evolution of Iberia, *Geol. Mag.*, *144*, 963–976, doi:10.1017/S0016756807003858.

Montes, A. D., J. R. Martínez-Catalán, and F. Bellido Mulas (2010), Role of the Ollo de Sapo massive felsic volcanism of NW Iberia in the Early Ordovician dynamics of northern Gondwana, *Gondwana Res.*, *17*(2–3), 363–376, doi:10.1016/j.gr.2009.09.001.

Moreno-Ventas, I., G. Rogers, and A. Castro (1995), The role of hybridization in the genesis of Hercynian granitoiels in the Gredos Massif, Spain: inferences from Sr-Nd isotopes, *Contrib. Mineral. Petrol.*, *120*, 137–149, doi:10.1007/BF00287111.

Murphy, J. B., and J. Dostal (2007), Continental mafic magmatism of different ages in the same terrane: Constraints on the evolution of an enriched mantle source, *Geology*, *35*(4), 335–338, doi:10.1130/G23072A.1.

Murphy, J. B., G. Gutiérrez-Alonso, J. Fernández-Suárez, and J. A. Braid (2008), Probing crustal and mantle lithosphere origin through Ordovician volcanic rocks along the Iberian passive margin of Gondwana, *Tectonophysics*, *461*(1–4), 166–180, doi:10.1016/j.tecto.2008.03.013.

Nance, R. D., G. Gutiérrez-Alonso, J. D. Keppie, U. Linnemann, J. B. Murphy, C. Quesada, R. A. Strachan, and N. H. Woodcock (2010), Evolution of the Rheic Ocean, *Gondwana Res.*, *17*(2–3), 194–222, doi:10.1016/j.gr.2009.08.001.

Neiva, A. M. R., I. S. Williams, J. M. F. Ramos, M. E. P. Gomes, M. M. V. G. Silva, and I. M. H. R. Antunes (2009), Geochemical and isotopic constraints on the petrogenesis of Early Ordovician granodiorite and Variscan two-mica granites from the Gouveia area, central Portugal, *Lithos*, *111*, 186–202, doi:10.1016/j.lithos.2009.01.005.

Orejana, D., C. Villaseca, C. Perez-Soba, J. A. Lopez-Garcia, and K. Billstrom (2009), The Variscan gabbros from the Spanish Central System: A case for crustal recycling in the sub-continental lithospheric mantle?, *Lithos*, *110*, 262–276, doi:10.1016/j.lithos.2009.01.003.

Orejana, D., C. Villaseca, R. A. Armstrong, and T. E. Jeffries (2011), Geochronology and trace element chemistry of zircon and garnet from granulite xenoliths: Constraints on the tectonothermal evolution of the lower crust under central Spain, *Lithos*, *124*, 103–116, doi:10.1016/j.lithos.2010.10.011.

Pearce, J. A., N. B. W. Harris, and A. G. Tindle (1984), Trace-element discrimination diagrams for the tectonic interpretation of granitic-rocks, *J. Petrol.*, *25*(4), 956–983.

Pérez-Estaún, A., et al. (1994), Crustal structure of the external variscides in northwest spain from deep seismic-reflection profiling, *Tectonophysics*, *232*(1–4), 91–118, doi:10.1016/0040-1951(94)90078-7.

Pérez-Estaún, A., and F. Bea (2004), Macizo Ibérico, in *Geología de España*, edited by J. A. Vera, pp. 19–230, SGE-IGME, Madrid.

Pinarelli, L., and A. Rottura (1995), Sr and Nd isotopic study and Rb-Sr geochronology of the Bejar granites, Iberian Massif, Spain, *Eur. J. Mineral.*, *7*(3), 577–589.

Pitcher, W. S. (1979), Nature, ascent and emplacement of granitic magmas, *J. Geol. Soc.*, *136*, 627–662, doi:10.1144/gsjgs.136.6.0627.

Rapp, R. P., T. Irifune, N. Shimizu, N. Nishiyama, M. D. Norman, and J. Inoue (2008), Subduction recycling of continental sediments and the origin of geochemically enriched reservoirs in the deep mantle, *Earth Planet. Sci. Lett.*, *271*(1–4), 14–23, doi:10.1016/j.epsl.2008.02.028.

Roberts, M. P., and J. D. Clemens (1993), Origin of high-potassium, calc-alkaline, i-type granitoids, *Geology*, *21*(9), 825–828, doi:10.1130/0091-7613(1993)021<0825:OOHPTA>2.3.CO;2.

Rodríguez, J., M. A. Cosca, J. I. G. Ibarguchi, and R. D. Dallmeyer (2003), Strain partitioning and preservation of $^{40}Ar/^{39}Ar$ ages during Variscan exhumation of a subducted crust (Malpica-Tui complex, NW Spain), *Lithos*, *70*(3–4), 111–139, doi:10.1016/S0024-4937(03)00095-1.

Schott, B., and H. Schmeling (1998), Delamination and detachment of a lithospheric root, *Tectonophysics*, *296*(3–4), 225–247, doi:10.1016/S0040-1951(98)00154-1.

Şengör, A. M. C. (1983), Gondwana and Gondwanaland: A discussion, *Geol. Rundsch.*, *72*(1), 397–400, doi:10.1007/BF01765917.

Şengör, A. M. C., and B. A. Natalin (1996), Turkic-type orogeny and its role in the making of the continental crust, *Annu. Rev. Earth Planet. Sci.*, *24*, 263–337, doi:10.1146/annurev.earth.24.1.263.

Solá, A. R., I. S. Williams, A. M. R. Neiva, and M. L. Ribeiro (2009), U-Th-Pb SHRIMP ages and oxygen isotope composition of zircon from two contrasting late Variscan granitoids, Nisa-Albuquerque batholith, SW Iberian Massif: Petrologic and regional implications, *Lithos*, *111*(3–4), 156–167, doi:10.1016/j.lithos.2009.03.045.

Song, X. Y., H. W. Qi, P. T. Robinson, M. F. Zhou, Z. M. Cao, and L. M. Chen (2008), Melting of the subcontinental lithospheric mantle by the Emeishan mantle plume; evidence from the basal alkaline basalts in Dongchuan, Yunnan, Southwestern China, *Lithos*, *100*(1–4), 93–111, doi:10.1016/j.lithos.2007.06.023.

Stampfli, G. M., and G. D. Borel (2002), A plate tectonic model for the Paleozoic and Mesozoic constrained by dynamic plate boundaries and restored synthetic oceanic isochrons, *Earth Planet. Sci. Lett.*, *196*(1–2), 17–33, doi:10.1016/S0012-821X(01)00588-X.

Sylvester, P. J. (1998), Post-collisional strongly peraluminous granites, *Lithos*, *45*(1–4), 29–44, doi:10.1016/S0024-4937(98)00024-3.

Valle Aguado, B. V., M. R. Azevedo, U. Schaltegger, J. R. M. Catalan, and J. Nolan (2005), U-Pb zircon and monazite geochronology of Variscan magmatism related to syn-convergence extension in Central Northern Portugal, *Lithos*, *82*(1–2), 169–184, doi:10.1016/j.lithos.2004.12.012.

Valverde-Vaquero, P. (1997), An integrated field, geochemical and U-Pb geochronological study of the SW Hermitage Flexure (Newfoundland Appalachians, Canada) and the Sierra de Guadarrama (Iberian Massif, Central Spain): A contribution to the understanding of the geological evolution of circum-Atlantic peri-Gondwana, Ph.D. thesis, 312 pp., Meml. Univ. of Newfoundland, St. John's, Newfoundland and Labrador, Canada.

Valverde-Vaquero, P., and G. R. Dunning (2000), New U-Pb ages for Early Ordovician magmatism in Central Spain, *J. Geol. Soc.*, *157*(1), 15–26, doi:10.1144/jgs.157.1.15.

Valverde-Vaquero, P., A. Cuesta-Fernández, G. Gallastegui, O. Suárez, L. G. Corretgé, and G. R. Dunning (1999), U–Pb dating of late-Variscan magmatism in the Cantabrian Zone (northern Spain), paper presented at EUG 10, Eur. Union of Geosci., Strasbourg, France, 28 Mar. to 1 Apr.

Valverde-Vaquero, P., M. A. Díez Balda, A. Díez Montes, W. Dörr, J. Escuder Viruete, E. González Clavijo, H. Maluski, L. R. Rodríguez-Fernández, F. Rubio, and P. Villar (2006), Timing of Variscan metamorphism and the Central Iberian paradox, *Geophys. Res. Abstr.*, *8*, 01309.

Valverde-Vaquero, P., T. Bento dos Santos, E. Clavijo, A. Díez Montes, L. Ribeiro, and R. Solá (2010), Geochronology and P-T-T Paths of the Berlengas Archipelago Rocks, W Portugal, paper presented at Goldschmidt 2010, Univ. of Tenn., Knoxville, 13–18 June.

Villaseca, C., H. Downes, C. Pin, and L. Barbero (1999), Nature and composition of the lower continental crust in central Spain and the granulite-granite linkage: Inferences from granulitic xenoliths, *J. Petrol.*, *40*(10), 1465–1496, doi:10.1093/petrology/40.10.1465.

Villaseca, C., F. Bellido, C. Perez-Soba, and K. Billstrom (2009), Multiple crustal sources for post-tectonic I-type granites in the Hercynian Iberian Belt, *Mineral. Petrol.*, *96*(3–4), 197–211, doi:10.1007/s00710-009-0057-2.

Viruete, J. E., R. Arenas, and J. R. M. Catalan (1994), Tectonothermal evolution associated with variscan crustal extension in the Tormes Gneiss Dome (NW Salamanca, Iberian Massif, Spain), *Tectonophysics*, *238*(1–4), 117–138, doi:10.1016/0040-1951(94)90052-3.

Watson, E. B., and T. M. Harrison (1983), Zircon saturation revisited: Temperature and composition effects in a variety of crustal magma types, *Earth Planet. Sci. Lett.*, *64*(2), 295–304, doi:10.1016/0012-821X(83)90211-X.

Weil, A. B., R. van der Voo, and B. A. van der Pluijm (2001), Oroclinal bending and evidence against the Pangea megashear: The Cantabria-Asturias arc (northern Spain), *Geology*, *29*(11), 991–994, doi:10.1130/0091-7613(2001)029<0991:OBAEAT>2.0.CO;2.

Weil, A., G. Gutiérrez-Alonso, and J. Conan (2010), New time constraints on lithospheric-scale oroclinal bending of the Ibero-Armorican Arc: A palaeomagnetic study of earliest Permian rocks from Iberia, *J. Geol. Soc.*, *167*, 127–143, doi:10.1144/0016-76492009-002.

Whitmeyer, S. J., and K. E. Karlstrom (2007), Tectonic model for the Proterozoic growth of North America, *Geosphere*, *3*(4), 220–259, doi:10.1130/GES00055.1.

Wiedenbeck, M., P. Alle, F. Corfu, W. L. Griffin, M. Meier, F. Oberli, A. Vonquadt, J. C. Roddick, and W. Speigel (1995), Three natural zircon standards for U-Th-Pb, Lu-Hf, trace-element and REE analyses, *Geostand. Newsl.*, *19*(1), 1–23, doi:10.1111/j.1751-908X.1995.tb00147.x.

Williamson, B. J., A. Shaw, H. Downes, and M. F. Thirlwall (1996), Geochemical constraints on the genesis of Hercynian two-mica leucogranites from the Massif Central, France, *Chem. Geol.*, *127*(1–3), 25–42, doi:10.1016/0009-2541(95)00105-0.

Wilson, M., E. R. Neumann, G. R. Davies, M. J. Timmerman, M. Heeremans, and B. T. Larsen (2004), Permo-Carboniferous magmatism and rifting in Europe: Introduction, in *Permo-Carboniferous Magmatism and Rifting in Europe*, edited by M. Wilson et al., *Geol. Soc. Spec. Publ.*, 223, 1–10.

Woodcock, N. H., N. J. Soper, and R. A. Strachan (2007), A Rheic cause for the Acadian deformation in Europe, *J. Geol. Soc.*, *164*, 1023–1036, doi:10.1144/0016-76492006-129.

Yenes, M., F. Alvarez, and G. Gutiérrez-Alonso (1999), Granite emplacement in orogenic compressional conditions: The La Alberca-Bejar granitic area (Spanish Central System, Variscan Iberian Belt), *J. Struct. Geol.*, *21*(10), 1419–1440, doi:10.1016/S0191-8141(99)00104-2.

Zeck, H. P., M. T. D. Wingate, and G. Pooley (2007), Ion microprobe U-Pb zircon geochronology of a late tectonic granitic-gabbroic rock complex within the Hercynian Iberian belt, *Geol. Mag.*, *144*(1), 157–177, doi:10.1017/S0016756806002652.

Ziegler, Z. A., and P. Dèzes (2006), Crustal evolution of Western and Central Europe, in *European Lithosphere Dynamics*, edited by D. G. Gee and R. A. Stephenson, pp. 43–56, Geol. Soc., London.

J. Fernández-Suárez, Departemento de Petrología y Geoquímica, Universidad Complutense and IGEO-CSIC, E-28040 Madrid, Spain.

M. P. Franco, J. C. Gonzalo, G. Gutiérrez-Alonso, and D. Pastor-Galán, Departamento de Geología, Universidad de Salamanca, Plaza de los Caídos s/n, E-37008 Salamanca, Spain. (gabi@usal.es)

T. E. Jeffries, Department of Mineralogy, Natural History Museum, London SW7 5BD, UK.

S. T. Johnston, School of Earth and Ocean Sciences, University of Victoria, PO Box 3055 STN CSC, Victoria, BC V8W 3P6, Canada.

J. B. Murphy, Department of Earth Science, St. Francis Xavier University, PO Box 5000, Antigonish, NS B2G 2W5, Canada.